A novel probe for phosphatidylinositol 4-phosphate reveals multiple pools beyond the Golgi

Gerald R.V. Hammond,[1] Matthias P. Machner,[2] and Tamas Balla[1]

[1]Program in Developmental Neuroscience and [2]Cell Biology and Metabolism Program, Eunice Kennedy Shriver National Institute of Child Health and Human Development, National Institutes of Health, Bethesda, MD 20892

Polyphosphoinositides are an important class of lipid that recruit specific effector proteins to organelle membranes. One member, phosphatidylinositol 4-phosphate (PtdIns4*P*) has been localized to Golgi membranes based on the distribution of lipid binding modules from PtdIns4*P* effector proteins. However, these probes may be biased by additional interactions with other Golgi-specific determinants. In this paper, we derive a new PtdIns4*P* biosensor using the PtdIns4*P* binding of SidM (P4M) domain of the secreted effector protein SidM from the bacterial pathogen *Legionella pneumophila*. PtdIns4*P* was necessary and sufficient for localization of P4M, which revealed pools of the lipid associated not only with the Golgi but also with the plasma membrane and Rab7-positive late endosomes/lysosomes. PtdIns4*P* distribution was determined by the localization and activities of both its anabolic and catabolic enzymes. Therefore, P4M reports a wider cellular distribution of PtdIns4*P* than previous probes and therefore will be valuable for dissecting the biological functions of PtdIns4*P* in its assorted membrane compartments.

Introduction

Eukaryotic organelles must maintain distinct protein and lipid compositions to preserve their unique functional identity, despite a process of vesicular transport that constantly exchanges the membrane between them (Roth, 2004). The polyphosphoinositides (PPIns) have emerged as a family of lipid molecules intimately associated with this process. PPIns are derivatives of the major structural phospholipid phosphatidylinositol (PtdIns) found in cytosolic membrane leaflets (Roth, 2004). The inositol head group can be phosphorylated at three distinct hydroxyls, generating three mono-, three bis-, and a single trisphosphorylated isomer. These PPIn isomers interact with hundreds of cellular proteins, regulating diverse processes at the membrane/cytosol interface, ranging from signal transduction to ion flux (Balla, 2013). The readily interchangeable phosphorylation status of the PtdIns head group by PPIn kinases and phosphatases enables restricted enrichment of these lipids on particular membrane compartments, even as bulk lipids move through vesicular transport (Roth, 2004).

Correspondence to Gerald R.V. Hammond: gerald.hammond@nih.gov

Abbreviations used in this paper: ANOVA, analysis of variance; FKBP, FK506 binding protein; FRB, FKBP12-rapamycin binding; iRFP, infra-RFP; nMDP, normalized mean deviation product; OSBP, oxysterol binding protein; P4M, PtdIns4*P* binding of SidM; PH, pleckstrin homology; PI4K, PtdIns 4-kinase; PIP5K, PtdIns4*P* 5-kinase; PJ, Pseudojanin; PM, plasma membrane; PPIn, polyphosphoinositide; PtdIns, phosphatidylinositol; PtdIns(3,5)P_2, PtdIns 3,5-bisphosphate; PtdIns3*P*, PtdIns 3-phosphate; PtdIns(4,5)P_2, PtdIns 4,5-bisphosphate; PtdIns4*P*, PtdIns 4-phosphate; ROI, region of interest; TIRF, total internal reflection fluorescence.

PtdIns 4-phosphate (PtdIns4*P*) was originally thought be a simple intermediate of the functionally prolific plasma membrane (PM) PPIn, PtdIns 4,5-bisphosphate (PtdIns(4,5)P_2; Balla, 2013); more recently, it has been found to be a key functional component of Golgi membranes (Graham and Burd, 2011). Early work in the yeast *Saccharomyces cerevisiae* identified mutants with compromised PtdIns4*P* synthesis as having defects in the early secretory pathway at the level of the Golgi apparatus (Hama et al., 1999; Walch-Solimena and Novick, 1999). Since then, many PtdIns4*P* effectors have been discovered, all of which appear to function on Golgi membranes, either in vesicle budding (Wang et al., 2003; Godi et al., 2004), nonvesicular lipid transport (Tóth et al., 2006; D'Angelo et al., 2007), or maintenance of Golgi structure (Dippold et al., 2009). Thus, PtdIns4*P* coordinates a diverse array of protein functions whose common feature is localization at the Golgi apparatus.

Although these data point to a rather restricted function at the Golgi, recent evidence has unearthed a more elaborate and less clearly defined picture for PtdIns4*P* function. First, several recent studies have found that the largest pool of the lipid—more than half of it at least—resides in the PM (Hammond et al.,

The Rockefeller University Press $30.00
J. Cell Biol.
www.jcb.org/cgi/doi/10.1083/jcb.201312072

2009; Sarkes and Rameh, 2010; Nakatsu et al., 2012). Second, PtdIns4*P* synthesis seems to span several membrane compartments. In mammals, PtdIns 4-kinase (PI4K) activity is encoded by four genes: *PI4KA* and *PI4KB* (*Sttp4* and *Pik1*, respectively, in *S. cerevisiae*; often referred to as type III enzymes after an antiquated classification of PtdIns kinase activities) as well as the evolutionarily distinct homologues *PI4K2A* and *PI4K2B* (with a single *Lsb6* orthologue in *S. cerevisiae*; Brown and Auger, 2011; Balla, 2013). Of these, *PI4KB* and *PI4K2A* have been implicated in Golgi PtdIns4*P* synthesis (Godi et al., 1999; Hama et al., 1999; Walch-Solimena and Novick, 1999; Wang et al., 2003; Polevoy et al., 2009; Minogue et al., 2010). However, *PI4K2A* has also been shown to function in endosomal/lysosomal traffic (Salazar et al., 2005; Minogue et al., 2006; Burgess et al., 2012; Jović et al., 2012), as has its homologue *PI4K2B* (Balla et al., 2002). Furthermore, a pool of PtdIns4*P* is produced on autophagosomes to support PtdIns(4,5)P_2 synthesis required for autophagic lysosome reformation (Rong et al., 2012), and some PtdIns4*P* has been reported on a subset of lysosomal membranes under normal conditions, which is required for lysosomal homeostasis (Sridhar et al., 2013). Finally, *PI4KA* has been shown to be responsible for PtdIns4*P* synthesis at the PM (Balla et al., 2008b; Nakatsu et al., 2012; Tan et al., 2014).

Can disparate synthesis of PtdIns4*P* on multiple membrane compartments be reconciled with its recruitment of effector proteins exclusively to Golgi membranes? Answering this question would require detection of the free lipid molecules available to recruit effector proteins in living cells. This has been attempted using fluorescent protein fusions of PtdIns4*P*-binding pleckstrin homology (PH) domains from Golgi effector proteins, which invariably localize to the Golgi in a PtdIns4*P*-dependent manner (Balla et al., 2005), apparently supporting a Golgi-selective enrichment of the lipid. A major caveat of this approach is that PH domains often exhibit tertiary intermolecular interactions that bias the probes' localization (Balla et al., 2000; Levine and Munro, 2002), i.e., PtdIns4*P* is not sufficient for membrane targeting. The PtdIns4*P*-binding Osh2p PH domain binds to the PM and Golgi in yeast (Roy and Levine, 2004) but localizes solely to the PM in mammalian cells, which could be interpreted as reflecting a relatively low concentration of available PtdIns4*P* at the Golgi. However, this probe also binds PM PtdIns(4,5)P_2 (Roy and Levine, 2004; Hammond et al., 2012). Immunocytochemical methods have detected PtdIns4*P* in both Golgi and PM (Hammond et al., 2009), but this technique is limited to fixed specimens and cannot answer the crucial question as to which pools of the lipid are available to recruit effector proteins.

Many bacterial pathogens have evolved secreted effector proteins with features that allow selective targeting of host cell membranes, which are then hijacked to support replication of the bacteria (Ham et al., 2011). The ability to bind or modify the PPIn head group is a common mechanism used by such proteins (Ham et al., 2011). We therefore sought to use the power of bacterial effector proteins as a tool to investigate PtdIns4*P* distribution in living cells. We focused on the SidM protein, secreted by the intracellular pathogen *Legionella pneumophila*. SidM is localized to *L. pneumophila*–containing vacuoles where its guanine nucleotide exchange factor and AMPylation activities stimulate Rab1 signaling, causing the recruitment of ER-derived materials (Machner and Isberg, 2007; Müller et al., 2010). *L. pneumophila*–containing vacuole recruitment is facilitated through binding to PtdIns4*P* by a unique PtdIns4*P* binding of SidM (P4M) domain (Brombacher et al., 2009). The P4M domain exhibits exquisite specificity and affinity for PtdIns4*P* in vitro (Brombacher et al., 2009; Schoebel et al., 2010) and is structurally distinct from the catalytic and Rab1-interacting activities (Schoebel et al., 2010; Zhu et al., 2010). The P4M domain from SidM is therefore an ideal candidate for an unbiased and sensitive biosensor for PtdIns4*P* in living cells.

Here, we show that PtdIns4*P* is necessary and sufficient for membrane targeting of P4M in living cells and that the probe detects readily accessible pools of the lipid in the Golgi, PM, and Rab7-positive endosomes/lysosomes. Each of the mammalian PI4Ks corresponds to at least one of these pools, and the PM and Golgi pools are accessible to the ER/Golgi-localized phosphatase Sac1.

Results

The P4M domain localizes to multiple membrane compartments in living cells

We expressed a GFP-conjugated P4M domain consisting of residues 546–647 of *L. pneumophila* SidM (Brombacher et al., 2009) in COS-7 cells and viewed the distribution by spinning-disk confocal microscopy. The probe was enriched on several membrane compartments (Fig. 1 A). Most prominent was a compact perinuclear compartment consistent with the Golgi apparatus. There was also a clear accumulation of peripheral labeling encompassing the entire cell, likely corresponding to the PM. Less obvious as a result of their smaller size and poorer contrast against the cytosolic background were smaller vesicular compartments enriched in P4M. These became more apparent when the entire volume of the cell was viewed as a maximum intensity projection (Fig. 1 A, middle). Time-lapse imaging revealed that these vesicular compartments were highly motile relative to the largely stationary Golgi and PM (Fig. 1 A, right; and Video 1).

A Golgi distribution of a PtdIns4*P*-binding biosensor is to be expected given the known localization of previous PH domain–based probes (Balla et al., 2005); indeed, one such probe—namely the PH domain from FAPP1 fused to GFP—colocalized with an infra-RFP (iRFP)–tagged P4M construct exclusively at the Golgi (Fig. 1 B). iRFP-P4M also colocalized with the mCherry-tagged PtdIns(4,5)P_2-binding PH domain from PLCδ1 (Fig. 1 B), which localizes only to the PM (Várnai and Balla, 1998). As expected, no colocalization was seen between the two disparately localized PH domain probes (Fig. 1 B). To improve membrane avidity of our novel probe, we made a tandem fusion of two P4M domains with GFP. Despite improved binding to the PM, Golgi membranes appeared highly distorted and compacted by the tandem construct (Fig. 1 C), so we did not characterize this probe further.

How faithfully does the localization of P4M reflect cellular accumulation of PtdIns4*P*? In vitro, P4M exhibits a remarkably

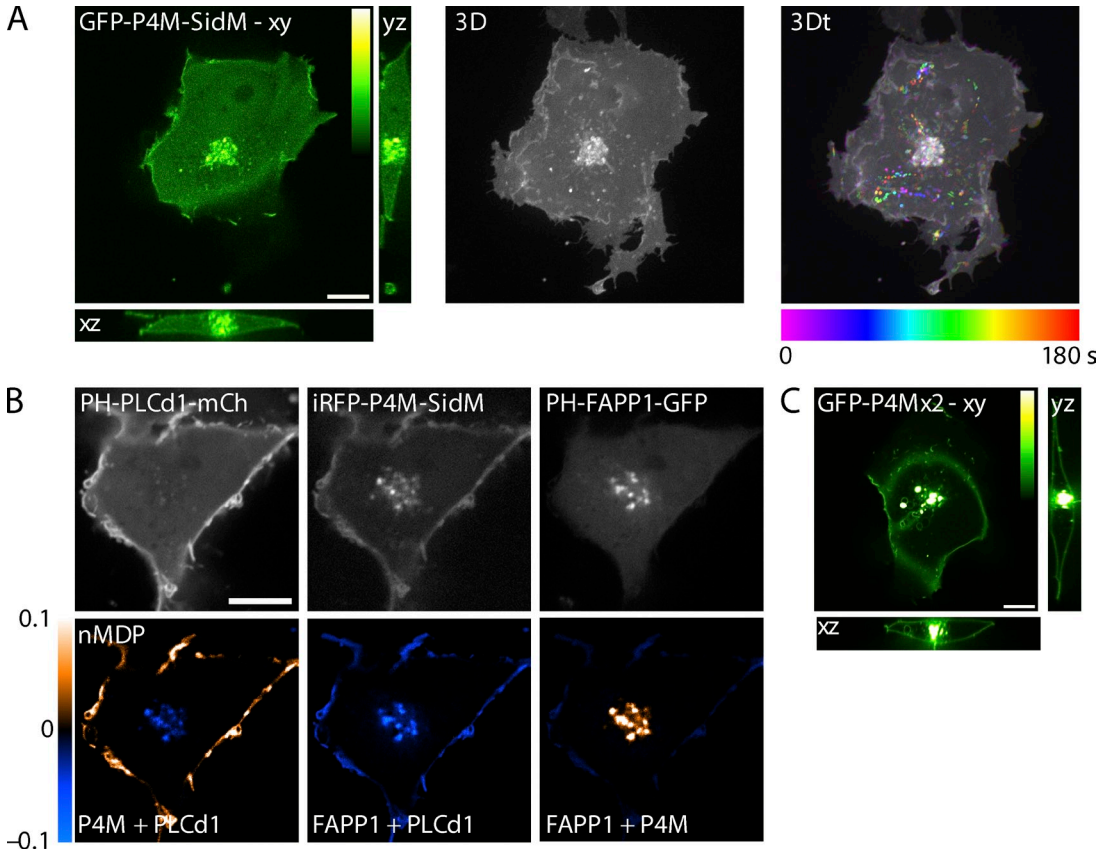

Figure 1. **Localization of fluorescent protein fusions of the P4M domain (residues 546–647) from *L. pneumophila* SidM/DrrA protein.** (A) GFP-P4M expressed in COS-7 cells and imaged on a spinning-disk confocal; shown are single confocal optical sections along the indicated axes, a 3D maximum intensity projection of 38 optical sections acquired at 0.2-µm intervals, or a color-coded temporal (3Dt) projection of 23 maximum intensity projections acquired at 8.15-s intervals. (B) Colocalization of the iRFP-tagged P4M domain with the PH domains from PLCδ1 and FAPP1. The color-coded images are normalized mean deviation product (nMDP) images of the indicated image pairs, showing the spatial distribution of colocalized pixels. mCh, mCherry. (C) Two P4M domains fused in tandem to GFP are shown as confocal optical sections along the indicated axes. Note the collapsed Golgi morphology. Bars, 10 µm.

specific, monogamous, and high-affinity binding to PtdIns4*P* (Brombacher et al., 2009; Schoebel et al., 2010). Nevertheless, the cell is a far more complex and diverse molecular environment than can be recapitulated in vitro, raising the possibility of additional interactions that could bias the probe's localization. We therefore set out to test whether PtdIns4*P* binding was necessary and sufficient to account for the localization of P4M in cells. We found that aldehyde fixation removed the membrane enrichment of P4M, precluding analysis of the probe's localization with endogenous markers detected using immunocytochemistry. Difficulties in preserving the localization of the probe during such procedures were not entirely unexpected because we previously reported the need for varied fixation and permeabilization conditions to preserve different PtdIns4*P*-containing membranes for immunofluorescence localization (Hammond et al., 2009). Furthermore, it has been reported that low-affinity interactions are not preserved during aldehyde fixation (Schmiedeberg et al., 2009), which may be further confounded in the case of P4M by the reaction of aldehydes with the primary amines in the arginine and lysine side chains required for PtdIns4*P* binding (Schoebel et al., 2010). We therefore focused our efforts on techniques applicable to live cells, as described in the remaining Results sections.

P4M domain binding to the Golgi is PtdIns4*P* dependent

To test whether binding to PtdIns4*P* was necessary for P4M targeting in cells, we used chemically induced recruitment of lipid-modifying enzymes to specific cellular compartments (Fili et al., 2006; Suh et al., 2006; Várnai et al., 2006). This system is based upon dimerization of the FK506 binding protein (FKBP) of 12 kD and the FKBP12-rapamycin–binding (FRB) domain from mammalian target of rapamycin induced by the cell-permeable immunosuppressant rapamycin (Brown et al., 1994). In our configuration, FRB is fused to a specific organelle resident motif, which recruits FKBP-conjugated PPIn kinases or phosphatases upon addition of rapamycin. This leads to rapid metabolism of the target PPIn specifically in the recruiting compartment (e.g., Fig. 2 A). This process can be followed by fluorescence microscopy in living cells by fusion of both constructs to fluorescent proteins. To deplete PtdIns4*P*, we used an mRFP- and FKBP-fused synthetic enzyme chimera Pseudojanin (PJ)-Sac (Hammond et al., 2012), which carries an active Sac domain from *S. cerevisiae Sac1* that dephosphorylates PtdIns4*P* to PtdIns (Guo et al., 1999).

We began by using PJ-Sac to deplete PtdIns4*P* from the Golgi to test the specificity of P4M's interaction with this organelle. In a previous study, we used FRB targeted to trans-Golgi

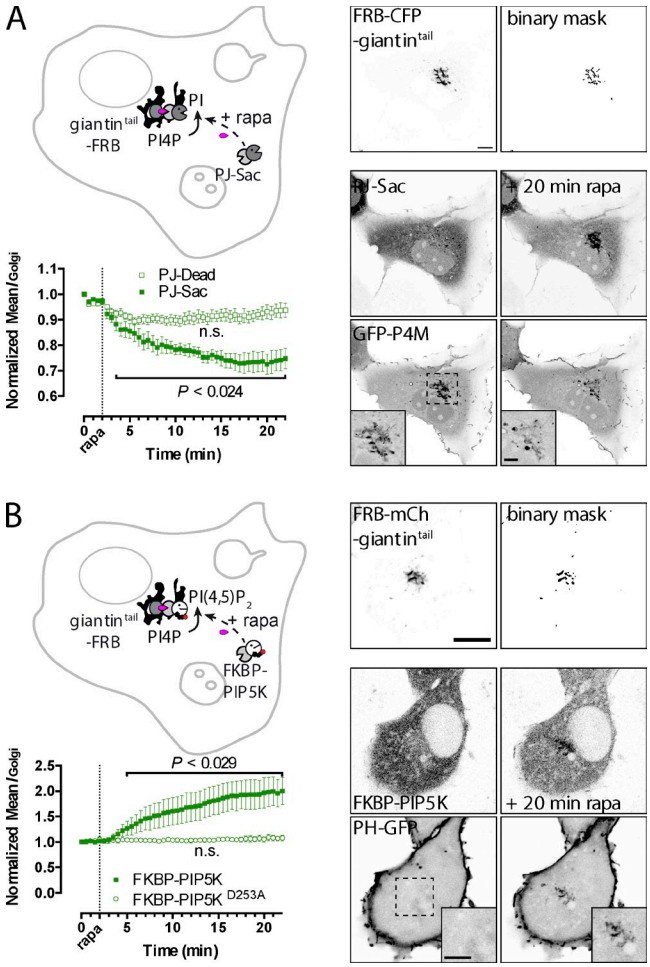

Figure 2. **P4M domain localization is PtdIns4*P* dependent at the Golgi, which contains low levels of PtdIns(4,5)P_2.** (A) Rapamycin (rapa)-induced recruitment of PJ-Sac to the FRB-tagged tail domain (residues 3,140–3,269) from human giantin (*GOLGB1*) induces dephosphorylation of PtdIns4*P* (PI4P) to PtdIns (PI), releasing GFP-P4M from the Golgi. No change is induced by the catalytically inactive PJ-Dead construct. Graphs show normalized intensity of GFP-P4M or PH-PLCδ1-GFP at the Golgi (defined by the FRB-giantin^{tail} mask) after treatment with 1 µM rapamycin. Data are grand means ± SEM of eight independent experiments. Significant ($P < 0.05$) changes are denoted as the largest p-value over the indicated range (two-way ANOVA; see Materials and methods). Images show representative cells with the Golgi localization of the FRB-mCherry-giantin^{tail} recruiter and its conversion to a binary mask for quantification of GFP-P4M fluorescence. Also shown is the localization of mRFP-tagged PJ-Sac and GFP-P4M before and after addition of 1 µM rapamycin. (B) Rapamycin-induced recruitment of FKBP-PIP5K to FRB-giantin^{tail} stimulates phosphorylation of PtdIns4*P* to produce PtdIns(4,5)P_2 (PI(4,5)P_2), recruiting PH-PLCδ1-GFP. No effect is observed for the catalytically inactive D253A mutant. Data are grand means of three or four independent experiments ± SEM. Insets depict an enlarged view of the regions depicted by hashed boxes. Bars: (main images) 10 µm; (insets) 5 µm.

membranes by TGN38 (Szentpetery et al., 2010). However, in recent experiments, we have found that recruitment of PPIn-modifying enzymes with TGN38 can lead to effects on lipids at the PM, consistent with the cycling of TGN38-containing membranes between the trans-Golgi network and the PM (Wakana et al., 2012). Instead, we used a construct using the C-terminal transmembrane domain of the cisternal Golgi-resident protein giantin, encoded by *GOLGB1* (Komatsu et al., 2010). This construct produced a tight localization to the Golgi (Fig. 2, A and B) and efficiently recruited PJ-Sac upon addition of rapamycin (Fig. 2 A and Video 2). This was followed by release of GFP-P4M from the Golgi region (Fig. 2 A and Video 2). No significant change in P4M localization was observed after recruitment of PJ-Dead (Hammond et al., 2012), a chimera with an inactivating mutation in the Sac domain, indicating that release of P4M from the Golgi required catalytic activity of Sac1 (Fig. 2 A). We conclude that P4M's localization to the Golgi is PtdIns4*P* dependent.

The finding that P4M recruitment to the Golgi is PtdIns4*P* specific is consistent with this lipid being the predominant PPIn at the Golgi. Conversion of PtdIns4*P* to PtdIns(4,5)P_2 has also been proposed at the Golgi (Godi et al., 1999), although the lipid is not detected there by the PH domain from PLCδ1 (Fig. 2 B; Várnai and Balla, 1998). Why not? Either Golgi PtdIns(4,5)P_2 levels are too low to be detected with PH-PLCδ1 or else tertiary interactions bias this probe's detection of PtdIns(4,5)P_2 exclusively to the PM (Balla et al., 2000). To discriminate between these possibilities, we recruited an FKBP-conjugated PtdIns4*P* 5-kinase (PIP5K), which converts PtdIns4*P* to PtdIns(4,5)P_2, to the Golgi; this manipulation caused significant accumulation of PH-PLCδ1 at the Golgi (Fig. 2 B and Video 3) but not when an inactivating mutation was introduced into PIP5K (Fig. 2 B). Therefore, PH-PLCδ1 does have the ability to detect PtdIns(4,5)P_2 in the Golgi, and we conclude that its failure to do so under normal conditions results from levels of the lipid being below the detection limit of this probe. This is consistent with PtdIns4*P* being the predominant PPIn at the Golgi.

As discussed in the introduction, several PH domain probes for PtdIns4*P* appear biased toward Golgi localization. For example, the PH domain from FAPP1 binds to both PtdIns4*P* and the small GTPase Arf1 (Levine and Munro, 2002; Godi et al., 2004); as a result, inhibition of GDP exchange on Arf1 by Brefeldin A inhibits Golgi binding of this domain (Balla et al., 2005). Indeed, we found that Brefeldin A decreased (but did not ablate) Golgi localization of PH-FAPP1 (Fig. 3 and Video 4). Conversely, in the same cell, the binding of P4M to the Golgi was slightly increased (Fig. 3 and Video 4), perhaps because of a small increase in free PtdIns4*P* levels after release of PH-FAPP1. Surprisingly, Brefeldin A treatment caused little dispersion of the P4M domain or the remaining PH-FAPP1 domain, despite causing dispersal of a cis/medial-Golgi marker derived from Mannosidase II (Fig. 3, C and D), indicating that this was not an artifact of P4M overexpression. The remaining P4M and FAPP1-PH remaining in the Golgi region likely represent trans-Golgi membranes, which are also enriched in PtdIns4*P* (Godi et al., 2004; Weixel et al., 2005) and that do not disperse with Brefeldin A treatment (Lippincott-Schwartz et al., 1989; Reaves and Banting, 1992). Regardless, this result demonstrates that, unlike several PH domain PtdIns4*P* probes, P4M is unbiased by interactions with Arf1.

P4M domain binding to the PM is PtdIns4*P* dependent

We next turned our attention to the specificity of P4M binding to the PM. Recruitment of PJ-Sac to the PM via a palmitoylated/myristoylated peptide from Lyn kinase caused the rapid release of P4M from the PM, without effect on the localization of the PtdIns(4,5)P_2 probe PH-PLCδ1 (Fig. 4 A and Video 5). This demonstrates that, unlike the previous PM PtdIns4*P* probe PH-Osh2p,

P4M binds the PM in a PtdIns4*P*-dependent, but PtdIns(4,5)P_2-independent, manner. Despite the role of PtdIns4*P* in PtdIns(4,5)P_2 synthesis, reduction of PtdIns4*P* levels has no appreciable effect on the PtdIns(4,5)P_2 probe, which is entirely consistent with our previous study exploring this very phenomenon (Hammond et al., 2012). Conversely, recruitment of an active INPP5 domain from INPP5E, which converts PtdIns(4,5)P_2 into PtdIns4*P*, would be expected to increase the levels of PtdIns4*P* in the PM. Indeed, depletion of PtdIns(4,5)P_2 caused the release of PH-PLCδ1, and the accompanying increase in PtdIns4*P* was reflected by augmented PM recruitment of P4M (Fig. 4 B and Video 6).

Depletion of both lipids from the PM with PJ, a chimera carrying both active Sac and INPP5E domains (Hammond et al., 2012) caused release of both P4M and PH-PLCδ1 from the PM (Fig. 4 C), whereas inactivating mutations in both phosphatases (PJ-Dead) produced no changes in the localization of either probe (Fig. 4 D). These observations lead us to the conclusion that P4M's interaction with PtdIns4*P* is both necessary and sufficient for its binding to the PM.

Previous studies have noted that the PH domain from oxysterol binding protein (OSBP), although predominately localized to the Golgi, can recognize PtdIns4*P* at the PM under conditions in which its concentration rises (Balla et al., 2005; Halaszovich et al., 2009), similar to our observations for P4M (Fig. 4 B). We therefore sought to compare the two domains. Given that PH-OSBP's PM localization is barely detectable in confocal microscopy (Balla et al., 2005), we turned to the quantitatively more sensitive total internal reflection fluorescence (TIRF) microscopy. When observed in TIRF, depletion of PM PtdIns4*P* with PJ-Sac caused similar significant drops in the intensity of both P4M and PH-OSBP tagged with GFP (Fig. 4 E). Conversion of PM PtdIns(4,5)P_2 to PtdIns4*P* caused an ∼10% increase in recruitment of PH-OSBP (although this was not statistically significant), whereas P4M was elevated significantly more, by ∼30% (Fig. 4 F). Taking these observations together, P4M thus represents a superior probe for PM PtdIns4*P* that the previously available PH domain probes from OSBP and Osh2p.

The P4M domain detects PtdIns4*P* on endosomes/lysosomes

Having established PtdIns4*P*-dependent binding to PM and Golgi membranes, it was important to identify the mysterious vesicular structures labeled by P4M, especially because these are not seen with other probes for PtdIns4*P*. Given PtdIns4*P*'s role in vesicular transport from the Golgi (Walch-Solimena and Novick, 1999; Wang et al., 2003; Godi et al., 2004), we initially suspected that these may represent secretory carriers. However, loading cells with LysoTracker green, which accumulates in acidic late endosomal and lysosomal compartments, revealed a surprisingly close association of P4M with motile, peripheral structures as well as more stationary objects closely apposed to the Golgi (Fig. 5 A and Video 7). Consistently, P4M-positive compartments also showed a tight overlap with Rab7 (Fig. 5 B), a marker of late endosomes and endosomes/lysosomes (Méresse et al., 1995). P4M showed some overlap with the early endosomal marker Rab5 (Bucci et al., 1992), although this was significantly less pronounced than with

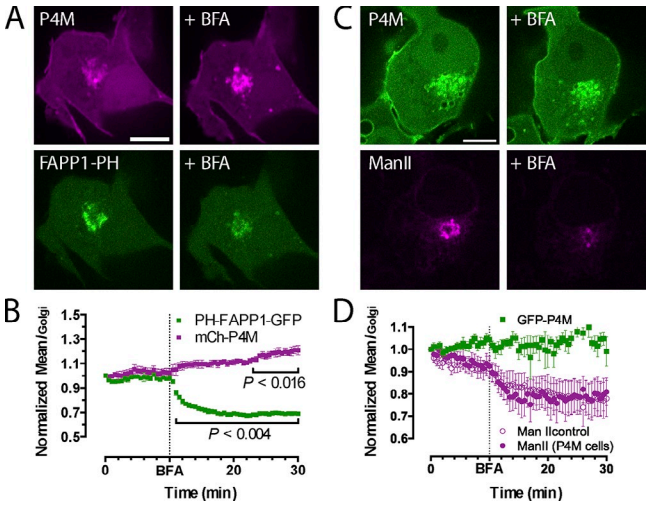

Figure 3. **P4M Golgi localization is independent of Arf1.** (A) COS-7 cells expressing mCherry-P4M and PH-FAPP1-GFP before and 20 min after the addition of 5 µg/ml Brefeldin A (BFA). (B) Normalized intensity of PH-FAPP1-GFP and mCherry (mCh)-P4M at the Golgi after treatment with 5 µM Brefeldin A. Data are grand means ± SEM of three independent experiments. Significant ($P < 0.05$) changes are denoted as the largest p-value over the indicated range (two-way ANOVA; see Materials and methods). (C) COS-7 cells expressing GFP-P4M and ManII$^{1–102}$–mKusabira Orange before and 20 min after the addition of 5 µg/ml Brefeldin A. (D) Normalized intensity of GFP-P4M and ManII$^{1–102}$–mKusabira Orange; data are means ± SEM of seven cells from two independent experiments. Bars, 10 µm.

Rab7 (Fig. 5 B). In contrast, the EEA1 FYVE domain, a probe for PtdIns 3-phosphate (PtdIns3*P*) known to be tightly associated with Rab5-positive early endosomes (Gillooly et al., 2000; Fili et al., 2006), showed a tight colocalization with Rab5 that was much stronger than with Rab7 (Fig. 5 C). Despite some overlap of both probes with Rab5, we did not observe colocalization of the EEA1 FYVE domain with P4M, which labeled distinct vesicular structures (Fig. 6 A).

P4M domain binding to the Rab7-positive compartments is PtdIns4*P* dependent

Does this endosomal/lysosomal P4M localization reveal a novel pool of PtdIns4*P* in this compartment? Careful dissection of the specificity of P4M binding was required to produce a satisfactory answer to this question because other PPIns, namely PtdIns3*P* and PtdIns 3,5-bisphosphate (PtdIns(3,5)P_2), have been reported on early endosomal and late endosomal/lysosomal compartments (Roth, 2004). Cotransfection of cells with the PtdIns3*P* reporter GFP-FYVE-EEA1 (Balla et al., 2000) revealed an exclusive localization compared with mCherry-P4M (Fig. 6 A and Video 8). Furthermore, addition of the PPIn 3-kinase inhibitor Wortmannin caused complete elimination of punctate FYVE domain labeling, with no effect on P4M distribution (Fig. 6 A and Video 8), as predicted by the lack of in vitro PtdIns3*P* binding by P4M (Brombacher et al., 2009; Schoebel et al., 2010). This observation also argues against P4M binding to PtdIns(3,5)P_2 because synthesis of this lipid, like PtdIns3*P*, depends on PPIn 3-kinase activity.

To address the PtdIns4*P* dependence of P4M recruitment to the endosomal/lysosomal compartment, we generated

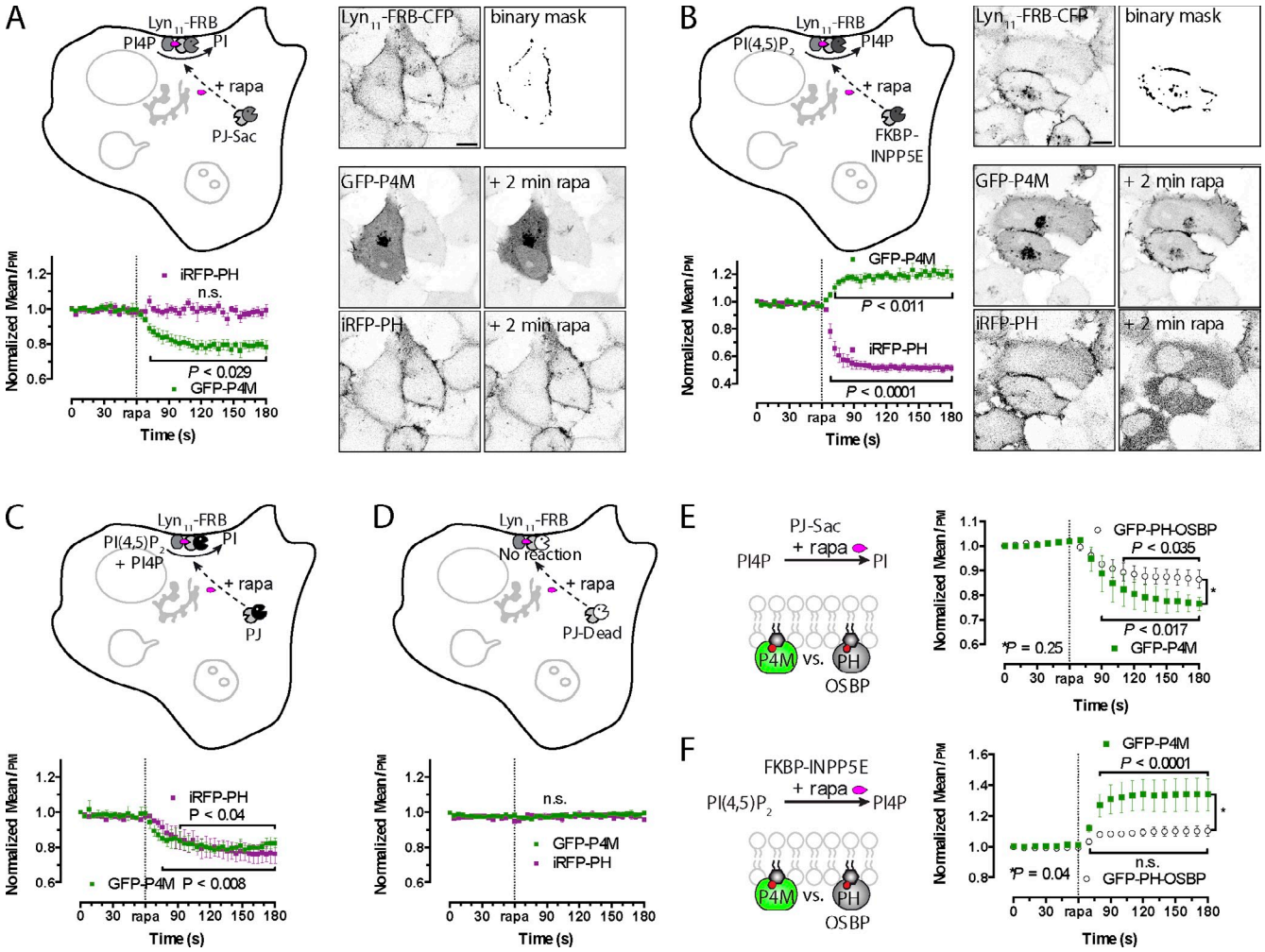

Figure 4. **P4M localization at the PM depends on PtdIns4*P*.** (A) Rapamycin (rapa)-induced recruitment of PJ-Sac to the PM via dimerization with FRB targeted to the PM causes depletion of PtdIns4*P* (PI4P) and release of GFP-P4M from the membrane, without effect on the PtdIns(4,5)P_2 (PI(4,5)P_2) probe iRFP-PH-PLCδ1. (B) Recruitment of an INPP5E domain to the PM causes breakdown of PtdIns(4,5)P_2 into PtdIns4*P*, causing release of iRFP-PH-PLCδ1 and increased PM binding of GFP-P4M. (C) PM recruitment of PJ (containing both Sac and INPP5E domains) causes breakdown of PtdIns(4,5)P_2 and PtdIns4*P* into PtdIns, resulting in release of both probes from the PM. (D) No effect on either probe is seen when catalytically inactive mutations in the Sac and INPP5E domains are introduced into PJ. (E and F) PM intensity of cells expressing either PtdIns4*P*-binding GFP-P4M or GFP-PH-OSBP during recruitment of PJ-Sac (E) or INPP5E (F) was measured by TIRF. Images show the FRB domain fused to CFP and the PM-targeted acylated Lyn_{11} peptide and the resulting binary masks used to measure PM intensity as well as the GFP-P4M and iRFP PH-PLCδ1 domains before and after enzyme recruitment with rapamycin. Graphs are from three (E) or four (A–D and F) independent experiments and are grand means ± SEM. Statistical significance (P < 0.05) is depicted over the indicated range (two-way ANOVA; see Materials and methods). n.s. = i.e., P > 0.05. Bars, 10 µm.

FRB-conjugated Rab7, which efficiently recruited PJ-Sac (Video 9) and caused the dissociation of P4M from the Rab7-positive membranes (Fig. 6 B and Video 9); in fact, almost all P4M-labeled vesicular structures were removed by this treatment, implying that Rab7-positive membranes are the major host compartment.

The *S. cerevisiae* Sac domain that we used in PJ-Sac has significant catalytic activity against PtdIns3*P* and PtdIns(3,5)P_2, both in vitro and in vivo (Guo et al., 1999). Therefore, as a control, we generated an FKBP-fused MTM1 (myotubularin 1) enzyme (Fili et al., 2006), which specifically hydrolyzes the 3-phosphate from PtdIns3*P* and PtdIns(3,5)P_2 but not other PPIns (Schaletzky et al., 2003). This enzyme did not produce an alteration in P4M localization at the Rab7-positive compartments (Fig. 6 C), firmly establishing the specific PtdIns4*P* dependence of P4M localization there.

As a further control for PJ-Sac specificity, we recruited both enzymes to PtdIns3*P*-rich early endosomes using an FRB fusion to Rab5 (Fig. 6 C). Whereas MTM1 caused a complete elimination of the PtdIns3*P* reporter GFP-FYVE-EEA1 from Rab5-positive membranes (Fig. 6 C), PJ-Sac had no significant effect (Fig. 6 C). Overall, these observations suggest that the catalytic preference of Sac for PtdIns4*P* is much greater than for PtdIns3*P*, at least in the configuration of PJ-Sac.

As a final test for the presence of PtdIns4*P* on Rab7-positive endosomal/lysosomal membranes, we reasoned that recruitment of the FKBP-PIP5K should generate PtdIns(4,5)P_2 there. Indeed, we saw recruitment of PH-PLCδ1 to Rab7-positive membranes after recruitment of the catalytically active, but not the inactive, PIP5K (Fig. 6 D and Video 10). Collectively, these observations firmly establish that PtdIns4*P* is generated in substantial quantities on late endosomal/lysosomal membranes.

Ectopic PtdIns4*P* synthesis is sufficient to recruit the P4M domain

The aforementioned experiments indicate that PtdIns4*P* is required to recruit P4M onto the membrane compartments labeled by it in live cells. However, for this to represent a definitive map of the cellular PtdIns4*P* distribution, we would need to confirm that PtdIns4*P* is sufficient for P4M recruitment. To test this, we sought a method to induce ectopic synthesis of PtdIns4*P* in cells. Infection by the plus-stranded RNA virus hepatitis C leads to replication of the virus on an ER-derived membranous web, to which the host cell's PI4KA enzyme is recruited, producing ectopic PtdIns4*P* (Berger et al., 2011; Reiss et al., 2011). The interaction depends on viral NS5A (nonstructural protein 5A), although the protein is not sufficient to recruit and activate endogenous PI4KA (Reiss et al., 2013). Consistent with this observation, we found that overexpression of an mCherry-tagged NS5A did not produce alterations in P4M distribution. However, coexpression of an active PI4KA enzyme with NS5A caused substantial accumulation of P4M on peripheral weblike membrane structures that colocalized with NS5A (Fig. 7). No such ectopic P4M accumulation was observed when the catalytically inactive D1957A mutant of PI4KA was expressed with NS5A (Fig. 7). We conclude that PtdIns4*P* is sufficient to drive the cellular distribution of P4M, which therefore likely reports all the substantial pools of accessible PtdIns4*P* within cells.

P4M domain localization corresponds to the cellular localization of PI4K

If these multiple organelle pools of PtdIns4*P* represent the cell's entire complement of this PPIn, does this correspond to the known localization of PtdIns4*P* metabolism? We sought to explore this through expression of the major PtdIns4*P* metabolic enzymes together with P4M. We first consider the PtdIns4*P*-synthesizing PI4Ks (Fig. 8 A): PI4KA has recently been shown to be recruited to the PM transiently and to rely on a multiprotein complex between the PM-anchored EFR3 proteins and the scaffold TTC7 (Baird et al., 2008; Nakatsu et al., 2012). Expression of these components in COS-7 cells together with P4M revealed a tight PM association of the palmitoylated EFR3B (as well as some internal membrane association), whereas TTC7B and PI4KA were mainly cytosolic (Fig. 8 A). Nonetheless, a small enrichment of both proteins was observed with EFR3, and PI4KA was the only enzyme to show any colocalization with P4M at the PM (Fig. 8 A). This is consistent with the dynamic recruitment of the kinase to the PM (Nakatsu et al., 2012) and its known role in PM PtdIns4*P* synthesis (Balla et al., 2008b).

More clearly defined was the localization of PI4KB, which, as expected (Godi et al., 1999; Hama et al., 1999; Walch-Solimena and Novick, 1999; Polevoy et al., 2009), localized exclusively to the Golgi, where it colocalized with P4M (Fig. 8 A). As for PI4K2A and PI4K2B, these exhibit a more scattered localization, with small vacuoles, peripheral vesicles, and a perinuclear accumulation that could correspond to either late endosomal/lysosomes or trans-Golgi membranes (Fig. 8 A). All of these distributions colocalized with a pool of membrane-bound P4M (Fig. 8 A) and are consistent with the reported endosomal/lysosomal and trans-Golgi localization of these enzymes (Balla et al., 2002;

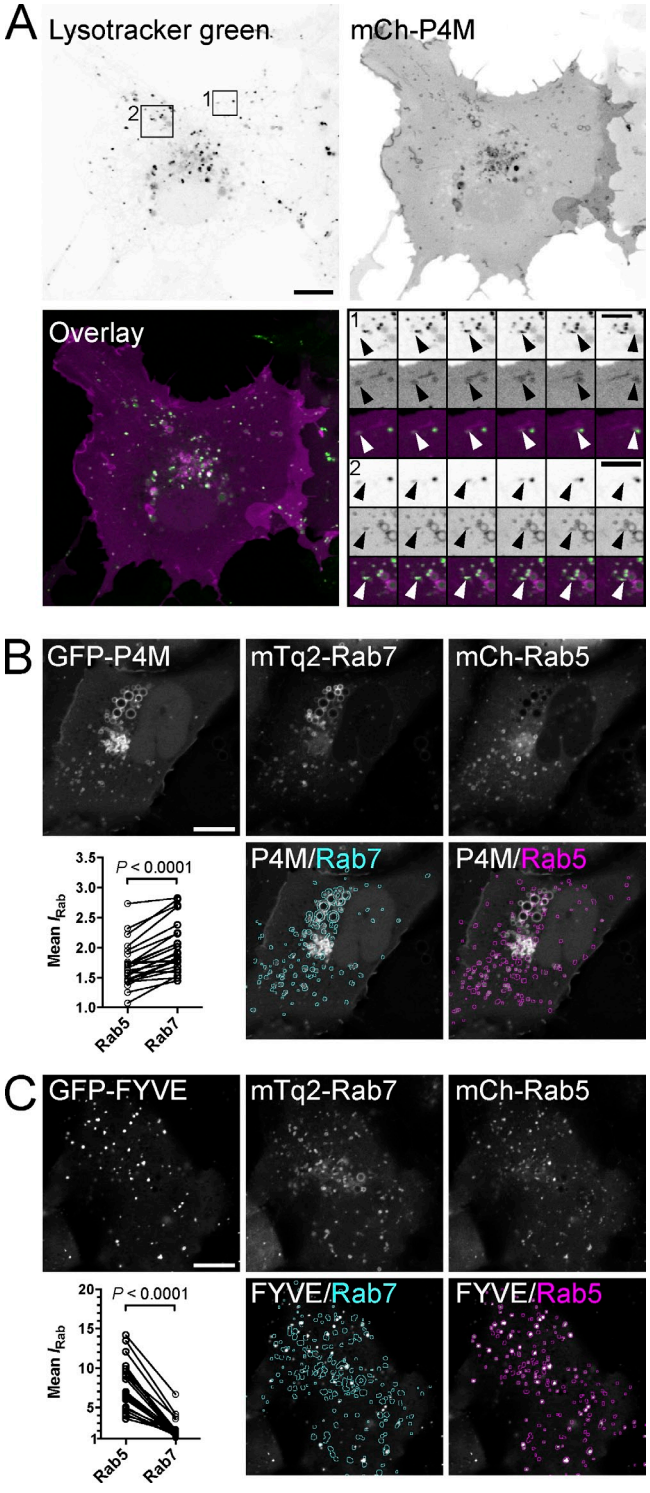

Figure 5. **P4M binds endosomes/lysosomes.** (A) COS-7 cells expressing mCherry (mCh)-tagged P4M were loaded with 100 nM LysoTracker green. The insets 1 and 2 are shown as a montage of images acquired at 3.9-s intervals showing motile, P4M, and LysoTracker-positive structures highlighted by the arrowheads. (B) COS-7 cells transfected with GFP-P4M, the late endosomal marker Rab7 (tagged with mTurquoise2 [mTq2]), and the early endosomal marker Rab5 (tagged with mCherry). A binary mask derived from the Rab7 and Rab5 images was used to calculate the relative intensity of the P4M signal associated with each compartment. The results from 24 cells are shown as a paired scatter plot. (C) As in B, except cells were transfected with the GFP-tagged FYVE domain from EEA1 as a marker of PtdIns3*P*. Bars: (main images) 10 µm; (insets) 5 µm. Statistics report the p-value from a paired Student's *t* test (see Materials and methods).

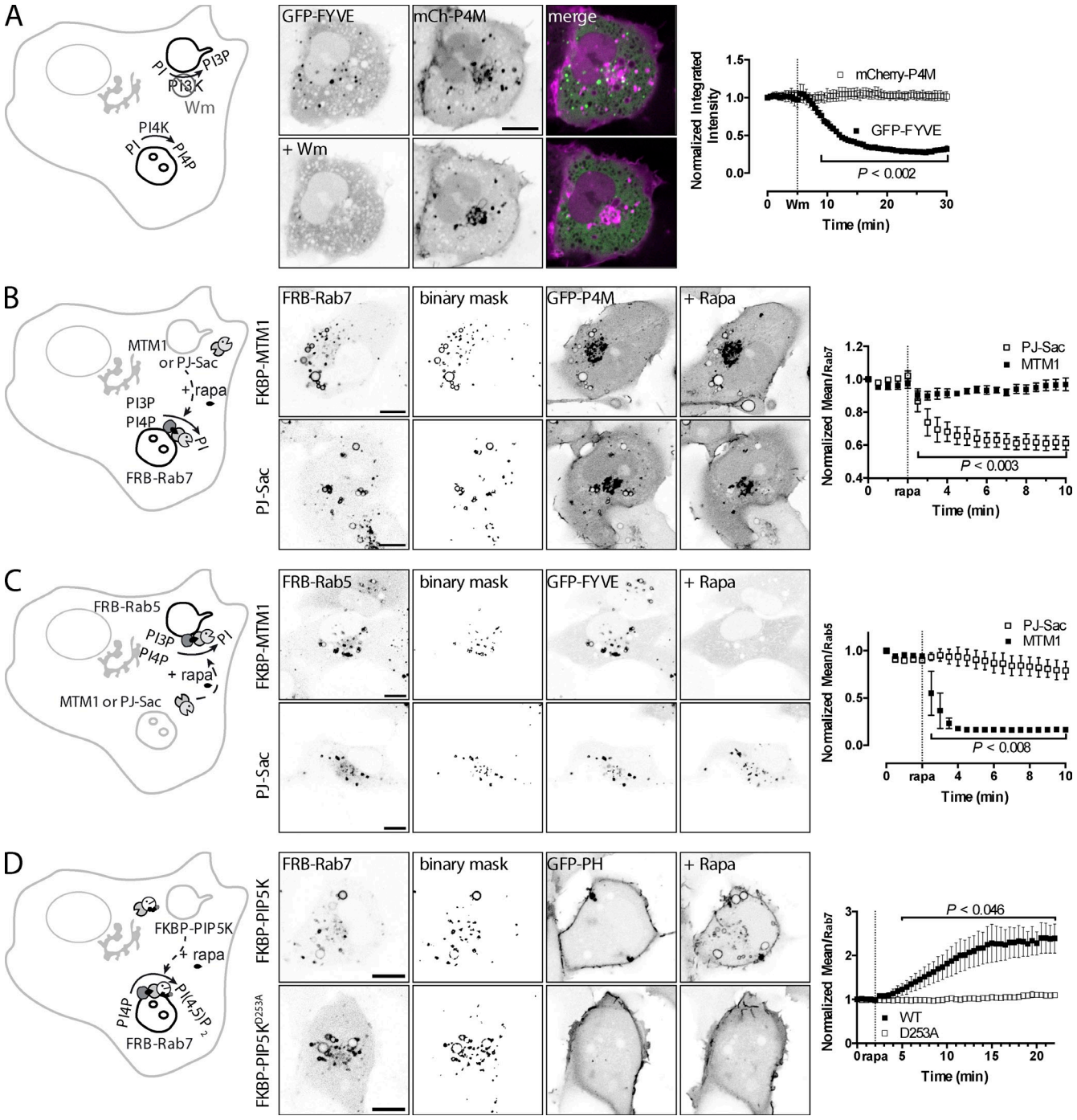

Figure 6. **P4M localization is dependent on endosomes/lysosomal PtdIns4*P*.** (A) COS-7 cells transfected with the PtdIns3*P* (PI3P) reporter GFP-FYVE-EEA1 and mCherry-P4M imaged by spinning-disk confocal microscopy during treatment with 100 nM wortmannin, a PtdIns 3-kinase (PI3K) inhibitor. (B) FRB targeted to late endosomes/lysosomes by fusion to Rab7 recruits lipid phosphatase PJ-Sac (active against PtdIns4*P*, PtdIns3*P*, and PtdIns(3,5)P_2) or MTM1 (active against PtdIns3*P* and PtdIns(3,5)P_2 but not PtdIns4*P*) in cells transfected with GFP-P4M. (C) FRB targeted to early endosomes by fusion to Rab5 recruits PJ-Sac or MTM1 in cells transfected with GFP-FYVE-EEA1. (D) FRB-Rab7 recruits a PIP5K or its catalytically inactive D253A mutant; the effect on PtdIns(4,5)P_2 generation is monitored with the PtdIns(4,5)P_2 reporter PH-PLCδ1-GFP. Graphs are grand means ± SEM from three independent experiments. Statistical significance (P < 0.05) is depicted over the indicated range (two-way ANOVA; see Materials and methods). n.s. = i.e., P > 0.05. rapa, rapamycin. Bars, 10 µm.

Wang et al., 2003; Salazar et al., 2005; Minogue et al., 2006; Minogue et al., 2010; Burgess et al., 2012; Jović et al., 2012). Altogether, these data reveal that all of the cellular PtdIns4*P* detected by P4M is accounted for by the localization of at least one of the PI4Ks, suggesting the enzymes each have an active role in PtdIns4*P* synthesis at distinct compartments.

PM and Golgi PtdIns4*P* is accessible to ER-localized Sac1

Turning to the catabolic side of PtdIns4*P* metabolism, we focused our attention on the major PtdIns4*P* phosphatase Sac1 (encoded by *SACM1L* in humans). This enzyme localizes predominantly to the ER in mammalians cells (Nemoto et al., 2000; Rohde et al.,

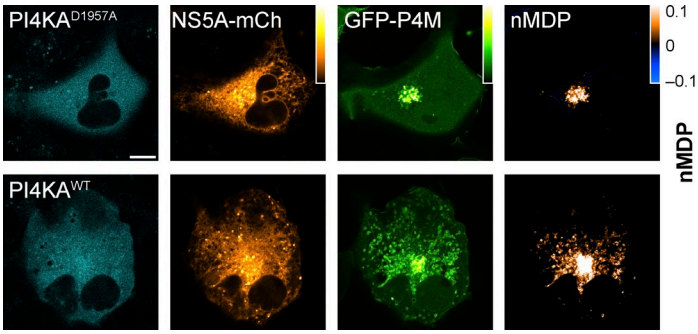

Figure 7. **GFP-P4M detects ectopic PtdIns4*P* synthesis in the ER driven by hepatitis C nonstructural protein 5A.** COS-7 cells transfected with GFP-P4M, NS5A-mCherry, and mTq2-tagged PI4KA wild type (WT) or its catalytically inactive D1957A mutant. Colocalization between GFP-P4M and NS5A-mCherry (mCh) is depicted in the nMDP images. The box and whisker plot shows the nMDP values for 30 cells (boxes denote the interquartile range with lines at the median; whiskers denote the 10th and 90th percentiles). The p-value was generated by a Mann–Whitney U test. Bar, 10 µm.

2003), where it is present at contact sites with both the PM (Stefan et al., 2011) and Golgi (Mesmin et al., 2013). It also traffics to the Golgi (Rohde et al., 2003) and can accumulate there during periods of cellular quiescence (Blagoveshchenskaya et al., 2008). We expressed an mCherry-tagged mouse Sac1 protein in COS-7 cells to investigate its possible colocalization with P4M. However, we discovered that overexpression of Sac1, despite its characteristic ER and Golgi localization, caused greatly reduced membrane localization of P4M compared with control cells expressing the catalytically inactive C389S mutant (Fig. 8 B), as assessed by the relative fluorescence intensity in membrane regions defined by Golgi, PM, or Rab7 marker proteins normalized to the total cellular fluorescence of the same cell (see Materials and methods). Localization of P4M to both the PM and Golgi compartments was significantly reduced, although the effect on Rab7-positive membranes was less clear (Fig. 8 B).

Is Golgi PtdIns4*P* broken down by ER-localized Sac1 at contact sites or by Golgi-localized Sac1? The Sac1–leucine-zipper alanine mutant cannot traffic to the Golgi (Blagoveshchenskaya et al., 2008) yet still degraded PM and Golgi PtdIns4*P*, if not to the same extent as the wild-type enzyme (Fig. 8 B). This implies that ER-localized Sac can access Golgi PtdIns4*P* pools as described recently (Mesmin et al., 2013), though much less efficiently than when Sac1 traffics into this organelle (Blagoveshchenskaya et al., 2008). The Sac1-K2A mutant accumulated in the Golgi (Rohde et al., 2003), although residual protein in the ER was probably responsible for depletion of PM PtdIns4*P* (Fig. 8 B). These observations support the recently described roles of ER- and Golgi-localized Sac1 in metabolizing both Golgi (Blagoveshchenskaya et al., 2008; Mesmin et al., 2013) and PM (Stefan et al., 2011) pools of this lipid.

Discussion

In this paper, we have described a new PtdIns4*P* probe based on the P4M domain from *L. pneumophila* SidM. We showed that PtdIns4*P* is both necessary and sufficient to account for the localization of the probe in live cells. P4M reveals a more extensive localization of PtdIns4*P* than detected with previous probes, reporting both PM and Golgi pools, as well as a pool associated with late endosomes and/or lysosomes. Although SidM has an exceptionally high ($\sim 10^{-8}$ M) affinity for PtdIns4*P* in vitro, the isolated P4M domain's affinity is substantially reduced (Brombacher et al., 2009). This was a distinct advantage for a cellular probe because its affinity seems well matched to the concentration of PtdIns4*P* in cells. This is indicated by P4M's ability to sense both increases and decreases in the lipid's abundance at the PM (Fig. 4, A and B). P4M thus represents an excellent PtdIns4*P* biosensor for use in live cells and represents a substantial improvement over previously described probes (Roy and Levine, 2004; Balla et al., 2005, 2008a; Halaszovich et al., 2009; Hammond et al., 2009). We believe this tool will be invaluable for interrogating the emerging roles of PtdIns4*P* in cellular traffic and homeostasis at multiple cellular locations.

This study confirms the substantial accumulation of PtdIns4*P* at the PM (Hammond et al., 2009; Sarkes and Rameh, 2010; Nakatsu et al., 2012) and reports a pool on the Rab7-positive late endosomal/lysosomal network—as predicted from functional studies of PI4Ks (Salazar et al., 2005; Minogue et al., 2006; Burgess et al., 2012; Jović et al., 2012; Sridhar et al., 2013). What does this tell us about the overall function of PtdIns4*P*? Its presence at comparable concentrations, as indicated by binding of P4M, in at least three organelle membranes means that a specific PtdIns4*P* binding protein could not distinguish these compartments based on lipid binding alone. However, PtdIns4*P* binding may assist in targeting proteins to specific organelles through interaction with other bona fide organelle-selective molecules; examples may include small GTPases, integral membrane proteins, or membrane curvature (Carlton and Cullen, 2005).

Our data do seem to support exclusive localization of PtdIns3*P* at Rab5-positive early endosomal membranes (Gillooly et al., 2000; Roth, 2004), which appeared devoid of either PtdIns4*P* or PtdIns(4,5)P_2. A novel probe for PtdIns(3,5)P_2 has recently been reported, which confirms this lipid's association with the endosomal/lysosomal network (Li et al., 2013). PtdIns(3,5)P_2 overlaps substantially with the early endosome–associated PtdIns3*P* pools (Li et al., 2013), which we reveal to be distinct from the PtdIns4*P*-containing endosomes (Fig. 6 A). Nonetheless, it will be intriguing to see whether late endosomal and lysosomal PtdIns(3,5)P_2 is present on the same compartments as PtdIns4*P* and what the functional relationship between these two lipid pools may be.

Our results also support the conclusion that most membrane PtdIns(4,5)P_2 is present at the PM (Várnai and Balla, 1998; Watt et al., 2002) because the PH-PLCδ1 probe localizes exclusively to this compartment but can detect PtdIns4*P*-containing membranes when ectopic PtdIns(4,5)P_2 synthesis is driven in them (Figs. 2 C and 6 D). However, PtdIns(4,5)P_2 is not a unique PPIn in the PM, which also contains levels of PtdIns4*P* far in excess of those required to support basal PtdIns(4,5)P_2 synthesis (Hammond

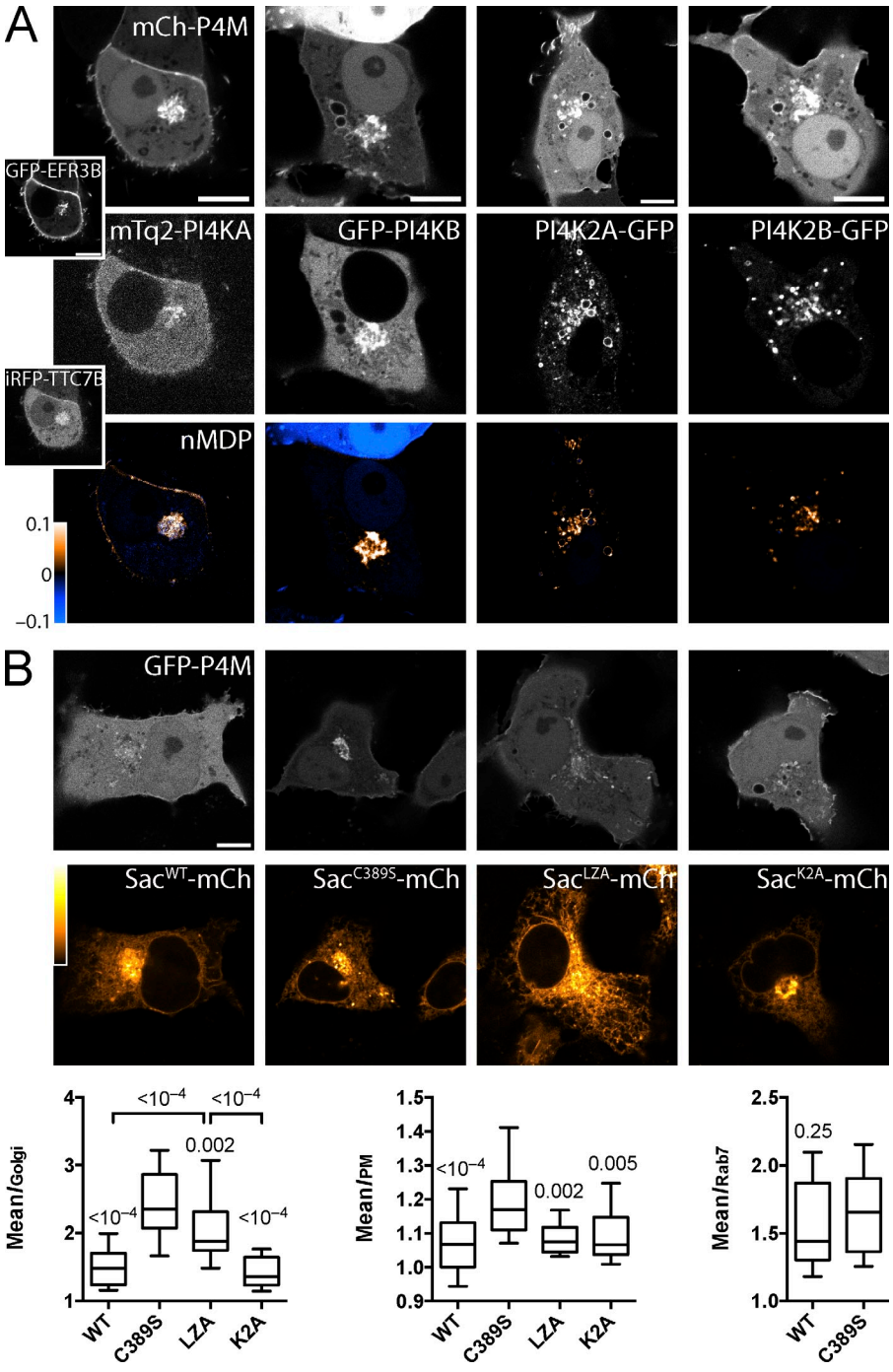

Figure 8. **GFP-P4M reveals pools of PtdIns4*P* accessible to all of the lipid's anabolic and catabolic enzymes.** (A) COS-7 cells transfected with mCherry (mCh)-P4M and a fluorescent protein conjugate of each of the four human PI4K isoforms. Cells expressing mTq2-tagged PI4KA and mCherry-P4M were cotransfected with GFP-EFR3B and iRFP-TTC7B (insets) that together recruit the kinase to the PM. Colocalizing pixels are highlighted in the nMDP imaged. (B) Cells transfected with GFP-P4M and mCherry-tagged Sac proteins: either wild type (WT), the C389S catalytically inactive mutant, leucine-zipper alanine (LZA) ER export–deficient mutant, or K2A Golgi retrieval–deficient mutant. The graphs show the relative P4M intensity at the Golgi, PM, and Rab7-positive compartments (box and whiskers as in Fig. 7; boxes denote the interquartile range with lines at the median; whiskers denote the 10th and 90th percentiles). The numbers above each group refer to the p-value (one-way ANOVA, 30 cells per group; see Materials and methods) compared with the C389S mutant or as indicated. Bars, 10 µm.

et al., 2012; Nakatsu et al., 2012). Although PtdIns(4,5)P_2 specifically supports a plethora of PM functions (Balla, 2013), it appears to cooperate with PtdIns4*P* to supply a polyanionic lipid requirement (Hammond et al., 2012), which together with ubiquitous anionic lipids such as phosphatidylserine give the PM a uniquely strong negative electrostatic charge compared with other membranes (Yeung et al., 2008). This negative electrostatic surface is recognized by several proteins containing polybasic motifs, which are therefore specifically recruited to the PM (Heo et al., 2006). However, the role played by PPIn in this electrostatic mechanism appears unique to the PM because endosomal membranes' weaker electrostatic potential seems to be satisfied by the presence of lipids such as phosphatidylserine (Yeung et al., 2008).

Drawing all of these observations together, it seems clear that PPIn metabolism is tightly restricted on specific membrane compartments. Multiple lipid kinases generate PtdIns4*P* at several cellular locations, suggesting a disparate function that is surely hinted at by the fact that, uniquely among PPIn kinases, PI4K activity has arisen twice by convergent evolution in the nonhomologous PI4K and PI4K2 families (Brown and Auger, 2011). What is the purpose of synthesizing the same PPIn on several organelle membranes? Recruitment of unique effector proteins to each compartment through tertiary, unique interactions

is one possibility (Carlton and Cullen, 2005). However, in over a decade of research, no specific PtdIns4*P* effectors that function outside of the Golgi have been discovered (Graham and Burd, 2011).

An intriguing alternative is revealed by recent observations that ER-localized Sac1 can act on PtdIns4*P* generated in the PM (Stefan et al., 2011) or Golgi (Mesmin et al., 2013). Lipid transfer domains that function at these junctions may shuttle PtdIns4*P* back to the ER for hydrolysis by Sac1, releasing energy from a gradient generated by PtdIns4*P* synthesis in the PM or Golgi membrane. This energy can be harnessed to drive transport of other lipid cargo against their chemical gradients (Kim et al., 2013; Mesmin et al., 2013). Therefore, PtdIns4*P* functions as a key component driving nonvesicular lipid transport. We speculate that such a mechanism may also operate at ER–late endosome contact sites mediated by the Rab7-associated ORP1L proteins (Rocha et al., 2009). Intriguingly, a similar PPIn-driven lipid transfer mechanism has also been proposed to function in α-tocopherol transport to the PM using PtdIns(4,5)P_2 (Kono et al., 2013). We suspect that the PPIn system has not arisen in eukaryotes as a simple membrane identity mechanism defining organelle compartments. Instead, we propose that the established roles of the PPIn in nonvesicular lipid transport and the recruitment of peripheral effector proteins are manifestations of the same functional principle: that PPIns are a eukaryotic mechanism that couples the energy of ATP hydrolysis (via PPIn synthesis) to the acquisition and maintenance of nonequilibrium organelle protein and lipid compositions.

In conclusion, we have characterized a novel, highly selective probe for PtdIns4*P* in living cells that reveals a more widespread distribution than could be detected with any single previous probe. This will facilitate interrogation of PtdIns4*P* function at multiple cellular locations, including the Golgi, PM, and late endosome/lysosome.

Materials and methods

Plasmids

All plasmids were constructed using the pEGFP-C1 or -N1 backbone (Takara Bio Inc.). When different fluors were used, EGFP was replaced with CFP, mTq2 (mTurquoise2; a gift from T. Gadella, University of Amsterdam, Amsterdam, Netherlands; Goedhart et al., 2012), mRFP (Campbell et al., 2002), mCherry (Shaner et al., 2004), or iRFP (Filonov et al., 2011).

The following cDNAs were amplified by PCR and subcloned into plasmids as follows: residues 546–647 from *L. pneumophila* SidM (available from GenBank under accession no. DQ845395), corresponding to the isolated P4M domain (Schoebel et al., 2010), were cloned into pEGFP-C1 (or spectral variants mCherry or iRFP) at BspEI and EcoRI sites. We also made a similar plasmid inserting the same P4M fragment at SalI and BamHI sites with a GGSASGLRS linker between GFP and the N terminus. This was used as a template to insert a second P4M insert at EcoRI and SalI sites with the same linker between GFP and the first P4M and a GGSAVDGGSASGLRS linker separating the tandem P4M domains. To generate FRB fused to canine Rab5 and Rab7 (a gift from R. Lodge, Institut de Recherches Cliniques de Montreal, Montreal, Quebec, Canada; Rojas et al., 2008), the entire coding regions were inserted at HindIII–KpnI sites of a modified piRFP-C1 vector containing the FRB domain (NCBI Nucleotide accession no. NM_004958; residues 2,021–2,113) flanked by GGAGA and GGSAGGSA linkers at the 5′ and 3′ ends, respectively, and inserted at BglII–HindIII sites. For pmCherry-C1-FKBP-MTM1, FKBP (NCBI Nucleotide accession no. NM_054014; residues 3–109) flanked by GAGGAARAAL and $(SAGG)_5$PRAQASNSA linkers at the 5′ and 3′ ends were inserted at NotI–SalI sites and MTM1(NCBI Nucleotide accession no. NM_000252) at SalI–BamHI. Hepatitis C NS5A (Budhu et al., 2007) was obtained from Addgene and inserted at HindIII–KpnI sites in pmCherry-N1. piRFP-N1-TTC7B (isolated from an EST that misses L53-A85 from exon 2; GenBank accession no. BQ426031) was inserted at NheI–SalI sites with a C-terminal GGSAGGSA linker with the iRFP. Constructs are available through Addgene. PI4KAv1 (NCBI Nucleotide accession no. NM_058004) was inserted at EcoRI–SalI sites of pmTq2-C1, and PI4KBv2 (NCBI Nucleotide accession no. NM_001198773) was inserted at XhoI–KpnI sites in pEGFP-C1. pEGFP-N1-EFR3B (NCBI Nucleotide accession no. NM_014971) was inserted at NheI–AgeI sites. Murine Sacm1l (NCBI Nucleotide accession no. NM_030692) was inserted at BglII–SalI sites in pmCherry-N1. Additional plasmids were obtained as follows: pEGFP-N1-PH-PLCδ1 (Várnai and Balla, 1998); pEGFP-N1-PH-FAPP1 and pEGFP-C1-PH-OSBP (Balla et al., 2005); PJ, its catalytic mutants, and pECFP-N1-Lyn_{11}-FRB (Hammond et al., 2012); pmRFP-FKBP-INPP5E (Várnai et al., 2006); pECFP-FRB-giantin$^{3,140–3,269}$ (a gift from T. Inoue, Johns Hopkins University School of Medicine, Baltimore, MD; Komatsu et al., 2010) or a pmCherry variant; pECFP-C1-FKBP-PIP5K (Suh et al., 2006); pmCherry-C1-Rab5 and -Rab7 (Rojas et al., 2008); GFP-FYVE-EEA1 (Balla et al., 2000); pEGFP-N1-PI4K2A (Jović et al., 2012); pEGFP-N1-PI4K2B (Balla et al., 2002); and piRFP-C1-PH-PLCδ1 (a gift from P. De Camilli, Yale School of Medicine, New Haven, CT; Idevall-Hagren et al., 2012).

Cell culture and transfection

COS-7 cells (CRL-1651; ATCC) were maintained in high glucose DMEM supplemented with L-glutamine and sodium pyruvate, 10% fetal bovine serum, 100 U/ml penicillin, and 100 µg/ml streptomycin (Life Technologies) at 37°C in 5% CO_2 and a humidified atmosphere and passaged with TrpLE (Life Technologies). Cells were seeded in 29-mm dishes with 20-mm #1 cover glass bottoms (In Vitro Scientific) at appropriate densities so that cells reached 50–100% confluence on the day of imaging. 20–26 h before imaging, cells were transfected in 1 ml Opti-MEM precomplexed for 20 min at room temperature with 3 µg Lipofectamine 2000 (Life Technologies) and 1 µg total DNA; the relative amounts of each construct were empirically determined based on the relative expression of each construct combination. After 4 h, complexes and Opti-MEM were removed and replaced with antibiotic-free medium.

Microscopy

For imaging, cells were placed in 800 µl of phenol red–free DMEM containing Hepes and L-glutamine (Life Technologies) and mounted on the microscope stage of inverted microscopes (see details in the following paragraph). When stimulated with compounds as described in the figure legends, 200 µl of the compound was freshly diluted before use at 5× final concentration and added to the dishes by bath application. All imaging was conducted at room temperature (~22°C).

Confocal imaging was performed on a laser-scanning confocal microscope (LSM 780; Carl Zeiss) operated with ZEN software (Carl Zeiss) using a 63×, 1.4 NA Plan Apochromatic objective lens. Respective laser lines for excitation and spectral detection windows for the fluorochromes were as follows: CFP and mTq2 (405 and 450–490 nm), GFP (488 and 508–543 nm), mRFP/mCherry (561 and 578–649 nm), and iRFP (633 and 650–758 nm). Combinations of all four fluors could be imaged on this system. To prevent cross talk, the spectrally well-resolved CFPs and iRFPs were excited and detected concurrently, whereas both GFPs and orange/RFPs were scanned sequentially. Spinning-disk confocal microscopy was performed on an inverted microscope (Eclipse Ti; Nikon) operated by Elements software (Nikon) and equipped with a 100×, 1.49 NA Plan Apochromatic objective lens, a 10,000-rpm spinning-disk scan head (CSU-X1; Yokogawa Corporation of America), and an electron-multiplying charge-coupled device camera (iXon DU897; Andor Technology). Excitation was with a fiber-coupled monolithic laser combiner (MLC-400; Agilent Technologies) equipped with 405-, 488-, 561-, and 640-nm lines. Appropriate GFP (500–550 nm), RFP (575–625 nm), or Cy5 (660–740 nm) emission filters (Chroma Technology Corp.) were used when sequentially imaging each fluorescent protein. A high speed piezo stage (City; Mad City Labs) was used to acquire z stacks. TIRF was performed on the same system using a second laser fiber output connected to a TIRF launch and a second camera port equipped with an electron-multiplying charge-coupled device camera (iXon DU897). Both microscope systems were equipped with reflected infrared light-driven focus-maintaining mechanisms that were used to ensure focus did not drift during acquisition or bath application of the agonist during time-lapse imaging. All data were acquired at 16-bit data depth. After linear scaling of the intensity, images were exported as 8-bit TIFFs for display in the figures.

Colocalization analysis

Colocalization between two fluorescent signals can be difficult to visualize by overlaying the two channels, especially when the proteins may have different intensities or different levels of contrast between the cellular structure of interest and the cytosolic background. This method is also inherently nonquantitative. Instead, we have used a modified implementation of the normalized mean deviation product (nMDP), a method that allows the quantitative visualization of colocalization between two fluorescent signals (Jaskolski et al., 2005) using a custom-written macro in Fiji (Schindelin et al., 2012). We manually produced regions of interest (ROIs) encompassing the entire cell to be measured (we found that automatic outlining with Sobel's kernels as originally proposed could not segment neighboring cells nor reliably pick out cells as a result of several contrasting regions in the fluorescent signal). The image was then normalized to the mean deviation of each pixel inside the ROI, i.e., the difference between maximum pixel intensity and the mean. After completing this operation for each channel, the nMDP was calculated as the pixel-by-pixel multiplication of the two images. Thus, regions in the two channels where intensities correlate will tend to produce larger, positive values, and regions where they differ produce smaller or more negative values. The overall index thus gives a statistically tractable measure of colocalization. For nMDP images shown in the paper, pixels in which both deviation products were below the mean, i.e., both negative (but producing a positive deviation product), were set to a value of 0 for clarity (i.e., black on the look-up table). Data were exported to Prism v6 (GraphPad Software), and all images were ranked by nMDP score. Images were selected for presentation that displayed clear morphological features and a high signal-to-noise ratio but that were close to the median score (and always fell within the interquartile range). Data failed a D'Agostino and Pearson omnibus normality test even after a natural logarithmic transformation, so we used the nonparametric Mann–Whitney U test for significant differences between control and experimental groups (Fig. 7).

Image intensity analysis

Image intensity measurements were made in Fiji. We have previously used a PM index based upon the ratio of intensity of a fluorescent protein in a membrane compartment relative to the cytosol to produce quantitative and statistically tractable measurements from our imaging data (Hammond et al., 2012). However, the large number of compartments labeled by P4M, and the motility of these compartments, made defining fixed ROI in the cytoplasm problematic: vesicular structures continuously moved in and out of these zones. Therefore, after manually defining ROIs containing whole cells, we normalized pixel intensity to the mean value of the whole cell at each time point. This corrects for both photobleaching and changes in protein concentration in the cytosol as levels at particular membranes change. To define the membrane compartment for measurement, we generated a binary mask of the compartment based on markers that were usually the FRB-conjugated recruiters (hence values are expressed as I_{Rab7} for intensity within the Rab7 mask, etc.). Masks were generated by an à trous wavelet decomposition at three length scales as previously described (Olivo-Marin, 2002) using a custom macro written for Fiji. In brief, this method smooths the raw image with Gaussian kernels of increasing pixel radii (i.e., length scales). These smoothed images are subtracted from the image smoothed at the preceding shorter length scale to produce detail images (the wavelet planes). The product of these three detail images was then calculated, and the modal pixel value (corresponding to featureless background) was subtracted before converting to a binary image. We found that that this approach could produce adequate, though imperfect, masks for each of the membrane compartments considered in this manuscript. We did not need to define a hard threshold for each wavelet as described by Olivo-Marin (2002), although the poorer signal to noise in images of the PM marker Lyn_{11} meant that we subjected these images to a 3 × 3 mean filter before applying the decomposition.

These masks thus produced an output of the underlying pixel intensity relative to the whole cell fluorescence (so a value of 1 indicated no enrichment on the membrane relative to the whole cell). Numbers are usually quoted as the mean pixel ratio. The one exception is for the experiment in Fig. 6 A, in which images of GFP-FYVE and mCheryy-P4M were used to generate their own masks. Here, the total (integrated) pixel ratio is quoted because the masking objects themselves could disappear. For time-lapse data, images were normalized to the pixel ratio at the start (time 0) because the relative change in each cell is the paramount measurement, as opposed to the absolute value of the pixel ratio in each compartment, which varies between cells. However, for the data in Figs. 5 (B and C) and 8 B, the absolute pixel ratio value for each cell is reported because comparisons between cells are made. Data were exported, graphed, and analyzed in Prism v6. The pixel ratio data were transformed with the natural logarithm to approximate a normal distribution and subjected to parametric tests. These were either Student's *t* test or two-way analysis of variance (ANOVA), with Bonferroni's post test applied to significantly varying datasets. For time-lapse data, all comparisons are to the time point immediately before the addition of compound. P-values are quoted on the graphs. Where not indicated, $P > 0.05$.

Online supplemental material

Videos 1–10 show time-lapse confocal imaging of a 3D maximum intensity projection of GFP-P4M (Video 1), the effects of PJ-Sac recruitment on the Golgi localization of GFP-P4M (Video 2), FKBP-PIP5K recruitment on the Golgi localization of PH-GFP (Video 3), 5 µg/ml Brefeldin A on the localization of PH-FAPP1-GFP and mCherry-P4M (Video 4), PJ-Sac recruitment on the PM localization of GFP-P4M and iRFP-PH-PLCδ1 (Video 5), FKBP-INPP5E recruitment on the PM localization of GFP-P4M and iRFP-PH-PLCδ1 (Video 6), mCherry-P4M colocalization with LysoTracker green–labeled endosomes/lysosomes (Video 7), the effects of Wortmannin on the localization of GFP-FYVE and mCherry-P4M (Video 8), PJ-Sac recruitment on the late endosomal/lysosomal localization of GFP-P4M (Video 9), and FKBP-PIP5K recruitment on the late endosomal/lysosomal localization of GFP-PH-PLCδ1 (Video 10). Online supplemental material is available at http://www.jcb.org/cgi/content/full/jcb.201312072/DC1. Additional data are available in the JCB DataViewer at http://dx.doi.org/10.1083/jcb.201312072.dv.

We are grateful to Pietro De Camilli, Takanari Inoue, Theodorus Gadella, and Robert Lodge for the kind gift of the plasmids detailed in the Materials and methods. Confocal and TIRF microscopy was performed in the Microscopy and Imaging Core of the Eunice Kennedy Shriver National Institute of Child Health and Human Development with the kind assistance of Drs. Vincent Schram and James Russel. We also thank Robin Irvine, Joseph Albanesi, Julie Brill, and Marko Jović for insightful comments on the manuscript.

The work was supported by the intramural program of the Eunice Kennedy Shriver National Institute of Child Health and Human Development of the National Institutes of Health.

The authors declare no competing financial interests.

Submitted: 16 December 2013
Accepted: 11 March 2014

References

Baird, D., C. Stefan, A. Audhya, S. Weys, and S.D. Emr. 2008. Assembly of the PtdIns 4-kinase Stt4 complex at the plasma membrane requires Ypp1 and Efr3. *J. Cell Biol.* 183:1061–1074. http://dx.doi.org/10.1083/jcb.200804003

Balla, A., G. Tuymetova, M. Barshishat, M. Geiszt, and T. Balla. 2002. Characterization of type II phosphatidylinositol 4-kinase isoforms reveals association of the enzymes with endosomal vesicular compartments. *J. Biol. Chem.* 277:20041–20050. http://dx.doi.org/10.1074/jbc.M111807200

Balla, A., G. Tuymetova, A. Tsiomenko, P. Várnai, and T. Balla. 2005. A plasma membrane pool of phosphatidylinositol 4-phosphate is generated by phosphatidylinositol 4-kinase type-III alpha: studies with the PH domains of the oxysterol binding protein and FAPP1. *Mol. Biol. Cell.* 16:1282–1295. http://dx.doi.org/10.1091/mbc.E04-07-0578

Balla, A., G. Tuymetova, B. Tóth, Z. Szentpetery, X. Zhao, Z.A. Knight, K. Shokat, P.J. Steinbach, and T. Balla. 2008a. Design of drug-resistant alleles of type-III phosphatidylinositol 4-kinases using mutagenesis and molecular modeling. *Biochemistry.* 47:1599–1607. http://dx.doi.org/10.1021/bi7017927

Balla, A., Y.J. Kim, P. Várnai, Z. Szentpetery, Z. Knight, K.M. Shokat, and T. Balla. 2008b. Maintenance of hormone-sensitive phosphoinositide pools in the plasma membrane requires phosphatidylinositol 4-kinase IIIalpha. *Mol. Biol. Cell.* 19:711–721. http://dx.doi.org/10.1091/mbc.E07-07-0713

Balla, T. 2013. Phosphoinositides: tiny lipids with giant impact on cell regulation. *Physiol. Rev.* 93:1019–1137. http://dx.doi.org/10.1152/physrev.00028.2012

Balla, T., T. Bondeva, and P. Várnai. 2000. How accurately can we image inositol lipids in living cells? *Trends Pharmacol. Sci.* 21:238–241. http://dx.doi.org/10.1016/S0165-6147(00)01500-5

Berger, K.L., S.M. Kelly, T.X. Jordan, M.A. Tartell, and G. Randall. 2011. Hepatitis C virus stimulates the phosphatidylinositol 4-kinase III alpha-dependent phosphatidylinositol 4-phosphate production that is essential for its replication. *J. Virol.* 85:8870–8883. http://dx.doi.org/10.1128/JVI.00059-11

Blagoveshchenskaya, A., F.Y. Cheong, H.M. Rohde, G. Glover, A. Knödler, T. Nicolson, G. Boehmelt, and P. Mayinger. 2008. Integration of Golgi trafficking and growth factor signaling by the lipid phosphatase SAC1. *J. Cell Biol.* 180:803–812. http://dx.doi.org/10.1083/jcb.200708109

Brombacher, E., S. Urwyler, C. Ragaz, S.S. Weber, K. Kami, M. Overduin, and H. Hilbi. 2009. Rab1 guanine nucleotide exchange factor SidM is a major phosphatidylinositol 4-phosphate-binding effector protein of *Legionella pneumophila*. *J. Biol. Chem.* 284:4846–4856. http://dx.doi.org/10.1074/jbc.M807505200

Brown, E.J., M.W. Albers, T.B. Shin, K. Ichikawa, C.T. Keith, W.S. Lane, and S.L. Schreiber. 1994. A mammalian protein targeted by G1-arresting rapamycin-receptor complex. *Nature*. 369:756–758. http://dx.doi.org/10.1038/369756a0

Brown, J.R., and K.R. Auger. 2011. Phylogenomics of phosphoinositide lipid kinases: perspectives on the evolution of second messenger signaling and drug discovery. *BMC Evol. Biol.* 11:4. http://dx.doi.org/10.1186/1471-2148-11-4

Bucci, C., R.G. Parton, I.H. Mather, H. Stunnenberg, K. Simons, B. Hoflack, and M. Zerial. 1992. The small GTPase rab5 functions as a regulatory factor in the early endocytic pathway. *Cell*. 70:715–728. http://dx.doi.org/10.1016/0092-8674(92)90306-W

Budhu, A., Y. Chen, J.W. Kim, M. Forgues, K. Valerie, C.C. Harris, and X.W. Wang. 2007. Induction of a unique gene expression profile in primary human hepatocytes by hepatitis C virus core, NS3 and NS5A proteins. *Carcinogenesis*. 28:1552–1560. http://dx.doi.org/10.1093/carcin/bgm075

Burgess, J., L.M. Del Bel, C.-I.J. Ma, B. Barylko, G. Polevoy, J. Rollins, J.P. Albanesi, H. Krämer, and J.A. Brill. 2012. Type II phosphatidylinositol 4-kinase regulates trafficking of secretory granule proteins in *Drosophila*. *Development*. 139:3040–3050. http://dx.doi.org/10.1242/dev.077644

Campbell, R.E., O. Tour, A.E. Palmer, P.A. Steinbach, G.S. Baird, D.A. Zacharias, and R.Y. Tsien. 2002. A monomeric red fluorescent protein. *Proc. Natl. Acad. Sci. USA*. 99:7877–7882. http://dx.doi.org/10.1073/pnas.082243699

Carlton, J.G., and P.J. Cullen. 2005. Coincidence detection in phosphoinositide signaling. *Trends Cell Biol.* 15:540–547. http://dx.doi.org/10.1016/j.tcb.2005.08.005

D'Angelo, G., E. Polishchuk, G. Di Tullio, M. Santoro, A. Di Campli, A. Godi, G. West, J. Bielawski, C.-C. Chuang, A.C. van der Spoel, et al. 2007. Glycosphingolipid synthesis requires FAPP2 transfer of glucosylceramide. *Nature*. 449:62–67. http://dx.doi.org/10.1038/nature06097

Dippold, H.C., M.M. Ng, S.E. Farber-Katz, S.-K. Lee, M.L. Kerr, M.C. Peterman, R. Sim, P.A. Wiharto, K.A. Galbraith, S. Madhavarapu, et al. 2009. GOLPH3 bridges phosphatidylinositol-4- phosphate and actomyosin to stretch and shape the Golgi to promote budding. *Cell*. 139:337–351. http://dx.doi.org/10.1016/j.cell.2009.07.052

Fili, N., V. Calleja, R. Woscholski, P.J. Parker, and B. Larijani. 2006. Compartmental signal modulation: Endosomal phosphatidylinositol 3-phosphate controls endosome morphology and selective cargo sorting. *Proc. Natl. Acad. Sci. USA*. 103:15473–15478. http://dx.doi.org/10.1073/pnas.0607040103

Filonov, G.S., K.D. Piatkevich, L.-M. Ting, J. Zhang, K. Kim, and V.V. Verkhusha. 2011. Bright and stable near-infrared fluorescent protein for in vivo imaging. *Nat. Biotechnol.* 29:757–761. http://dx.doi.org/10.1038/nbt.1918

Gillooly, D.J., I.C. Morrow, M. Lindsay, R. Gould, N.J. Bryant, J.M. Gaullier, R.G. Parton, and H. Stenmark. 2000. Localization of phosphatidylinositol 3-phosphate in yeast and mammalian cells. *EMBO J.* 19:4577–4588. http://dx.doi.org/10.1093/emboj/19.17.4577

Godi, A., P. Pertile, R. Meyers, P. Marra, G. Di Tullio, C. Iurisci, A. Luini, D. Corda, and M.A. De Matteis. 1999. ARF mediates recruitment of PtdIns-4-OH kinase-beta and stimulates synthesis of PtdIns(4,5)P2 on the Golgi complex. *Nat. Cell Biol.* 1:280–287. http://dx.doi.org/10.1038/12993

Godi, A., A. Di Campli, A. Konstantakopoulos, G. Di Tullio, D.R. Alessi, G.S. Kular, T. Daniele, P. Marra, J.M. Lucocq, and M.A. De Matteis. 2004. FAPPs control Golgi-to-cell-surface membrane traffic by binding to ARF and PtdIns(4)P. *Nat. Cell Biol.* 6:393–404. http://dx.doi.org/10.1038/ncb1119

Goedhart, J., D. von Stetten, M. Noirclerc-Savoye, M. Lelimousin, L. Joosen, M.A. Hink, L. van Weeren, T.W.J. Gadella Jr., and A. Royant. 2012. Structure-guided evolution of cyan fluorescent proteins towards a quantum yield of 93%. *Nat. Commun.* 3:751. http://dx.doi.org/10.1038/ncomms1738

Graham, T.R., and C.G. Burd. 2011. Coordination of Golgi functions by phosphatidylinositol 4-kinases. *Trends Cell Biol.* 21:113–121. http://dx.doi.org/10.1016/j.tcb.2010.10.002

Guo, S., L.E. Stolz, S.M. Lemrow, and J.D. York. 1999. SAC1-like domains of yeast SAC1, INP52, and INP53 and of human synaptojanin encode polyphosphoinositide phosphatases. *J. Biol. Chem.* 274:12990–12995. http://dx.doi.org/10.1074/jbc.274.19.12990

Halaszovich, C.R., D.N. Schreiber, and D. Oliver. 2009. Ci-VSP is a depolarization-activated phosphatidylinositol-4,5-bisphosphate and phosphatidylinositol-3,4,5-trisphosphate 5′-phosphatase. *J. Biol. Chem.* 284:2106–2113. http://dx.doi.org/10.1074/jbc.M803543200

Ham, H., A. Sreelatha, and K. Orth. 2011. Manipulation of host membranes by bacterial effectors. *Nat. Rev. Microbiol.* 9:635–646. http://dx.doi.org/10.1038/nrmicro2602

Hama, H., E.A. Schnieders, J. Thorner, J.Y. Takemoto, and D.B. DeWald. 1999. Direct involvement of phosphatidylinositol 4-phosphate in secretion in the yeast *Saccharomyces cerevisiae*. *J. Biol. Chem.* 274:34294–34300. http://dx.doi.org/10.1074/jbc.274.48.34294

Hammond, G.R.V., G. Schiavo, and R.F. Irvine. 2009. Immunocytochemical techniques reveal multiple, distinct cellular pools of PtdIns4P and PtdIns(4,5)P(2). *Biochem. J.* 422:23–35. http://dx.doi.org/10.1042/BJ20090428

Hammond, G.R.V., M.J. Fischer, K.E. Anderson, J. Holdich, A. Koteci, T. Balla, and R.F. Irvine. 2012. PI4P and PI(4,5)P2 are essential but independent lipid determinants of membrane identity. *Science*. 337:727–730. http://dx.doi.org/10.1126/science.1222483

Heo, W.D., T. Inoue, W.S. Park, M.L. Kim, B.O. Park, T.J. Wandless, and T. Meyer. 2006. PI(3,4,5)P3 and PI(4,5)P2 lipids target proteins with polybasic clusters to the plasma membrane. *Science*. 314:1458–1461. http://dx.doi.org/10.1126/science.1134389

Idevall-Hagren, O., E.J. Dickson, B. Hille, D.K. Toomre, and P. De Camilli. 2012. Optogenetic control of phosphoinositide metabolism. *Proc. Natl. Acad. Sci. USA*. 109:E2316–E2323. http://dx.doi.org/10.1073/pnas.1211305109

Jaskolski, F., C. Mulle, and O.J. Manzoni. 2005. An automated method to quantify and visualize colocalized fluorescent signals. *J. Neurosci. Methods*. 146:42–49. http://dx.doi.org/10.1016/j.jneumeth.2005.01.012

Jović, M., M.J. Kean, Z. Szentpetery, G. Polevoy, A.-C. Gingras, J.A. Brill, and T. Balla. 2012. Two phosphatidylinositol 4-kinases control lysosomal delivery of the Gaucher disease enzyme, β-glucocerebrosidase. *Mol. Biol. Cell*. 23:1533–1545. http://dx.doi.org/10.1091/mbc.E11-06-0553

Kim, Y.J., M.-L.G. Hernandez, and T. Balla. 2013. Inositol lipid regulation of lipid transfer in specialized membrane domains. *Trends Cell Biol.* 23:270–278. http://dx.doi.org/10.1016/j.tcb.2013.01.009

Komatsu, T., I. Kukelyansky, J.M. McCaffery, T. Ueno, L.C. Varela, and T. Inoue. 2010. Organelle-specific, rapid induction of molecular activities and membrane tethering. *Nat. Methods*. 7:206–208. http://dx.doi.org/10.1038/nmeth.1428

Kono, N., U. Ohto, T. Hiramatsu, M. Urabe, Y. Uchida, Y. Satow, and H. Arai. 2013. Impaired α-TTP-PIPs interaction underlies familial vitamin E deficiency. *Science*. 340:1106–1110. http://dx.doi.org/10.1126/science.1233508

Levine, T.P., and S. Munro. 2002. Targeting of Golgi-specific pleckstrin homology domains involves both PtdIns 4-kinase-dependent and -independent components. *Curr. Biol.* 12:695–704. http://dx.doi.org/10.1016/S0960-9822(02)00779-0

Li, X., X. Wang, X. Zhang, M. Zhao, W.L. Tsang, Y. Zhang, R.G.W. Yau, L.S. Weisman, and H. Xu. 2013. Genetically encoded fluorescent probe to visualize intracellular phosphatidylinositol 3,5-bisphosphate localization and dynamics. *Proc. Natl. Acad. Sci. USA*. 110:21165–21170. http://dx.doi.org/10.1073/pnas.1311864110

Lippincott-Schwartz, J., L.C. Yuan, J.S. Bonifacino, and R.D. Klausner. 1989. Rapid redistribution of Golgi proteins into the ER in cells treated with brefeldin A: evidence for membrane cycling from Golgi to ER. *Cell*. 56:801–813. http://dx.doi.org/10.1016/0092-8674(89)90685-5

Machner, M.P., and R.R. Isberg. 2007. A bifunctional bacterial protein links GDI displacement to Rab1 activation. *Science*. 318:974–977. http://dx.doi.org/10.1126/science.1149121

Méresse, S., J.P. Gorvel, and P. Chavrier. 1995. The rab7 GTPase resides on a vesicular compartment connected to lysosomes. *J. Cell Sci.* 108:3349–3358.

Mesmin, B., J. Bigay, J. Moser von Filseck, S. Lacas-Gervais, G. Drin, and B. Antonny. 2013. A four-step cycle driven by PI(4)P hydrolysis directs sterol/PI(4)P exchange by the ER-Golgi tether OSBP. *Cell*. 155:830–843. http://dx.doi.org/10.1016/j.cell.2013.09.056

Minogue, S., M.G. Waugh, M.A. De Matteis, D.J. Stephens, F. Berditchevski, and J.J. Hsuan. 2006. Phosphatidylinositol 4-kinase is required for endosomal trafficking and degradation of the EGF receptor. *J. Cell Sci.* 119:571–581. http://dx.doi.org/10.1242/jcs.02752

Minogue, S., K.M.E. Chu, E.J. Westover, D.F. Covey, J.J. Hsuan, and M.G. Waugh. 2010. Relationship between phosphatidylinositol 4-phosphate synthesis, membrane organization, and lateral diffusion of PI4KIIalpha at the trans-Golgi network. *J. Lipid Res.* 51:2314–2324. http://dx.doi.org/10.1194/jlr.M005751

Müller, M.P., H. Peters, J. Blümer, W. Blankenfeldt, R.S. Goody, and A. Itzen. 2010. The *Legionella* effector protein DrrA AMPylates the membrane traffic regulator Rab1b. *Science*. 329:946–949. http://dx.doi.org/10.1126/science.1192276

Nakatsu, F., J.M. Baskin, J. Chung, L.B. Tanner, G. Shui, S.Y. Lee, M. Pirruccello, M. Hao, N.T. Ingolia, M.R. Wenk, and P. De Camilli. 2012. PtdIns4P synthesis by PI4KIIIα at the plasma membrane and its impact on plasma membrane identity. *J. Cell Biol.* 199:1003–1016. http://dx.doi.org/10.1083/jcb.201206095

Nemoto, Y., B.G. Kearns, M.R. Wenk, H. Chen, K. Mori, J.G. Alb Jr., P. De Camilli, and V.A. Bankaitis. 2000. Functional characterization of a mammalian Sac1 and mutants exhibiting substrate-specific defects in phosphoinositide phosphatase activity. *J. Biol. Chem.* 275:34293–34305. http://dx.doi.org/10.1074/jbc.M003923200

Olivo-Marin, J.-C. 2002. Extraction of spots in biological images using multiscale products. *Pattern Recognit.* 35:1989–1996. http://dx.doi.org/10.1016/S0031-3203(01)00127-3

Polevoy, G., H.-C. Wei, R. Wong, Z. Szentpetery, Y.J. Kim, P. Goldbach, S.K. Steinbach, T. Balla, and J.A. Brill. 2009. Dual roles for the *Drosophila* PI 4-kinase four wheel drive in localizing Rab11 during cytokinesis. *J. Cell Biol.* 187:847–858. http://dx.doi.org/10.1083/jcb.200908107

Reaves, B., and G. Banting. 1992. Perturbation of the morphology of the trans-Golgi network following Brefeldin A treatment: redistribution of a TGN-specific integral membrane protein, TGN38. *J. Cell Biol.* 116:85–94. http://dx.doi.org/10.1083/jcb.116.1.85

Reiss, S., I. Rebhan, P. Backes, I. Romero-Brey, H. Erfle, P. Matula, L. Kaderali, M. Poenisch, H. Blankenburg, M.-S. Hiet, et al. 2011. Recruitment and activation of a lipid kinase by hepatitis C virus NS5A is essential for integrity of the membranous replication compartment. *Cell Host Microbe*. 9:32–45. http://dx.doi.org/10.1016/j.chom.2010.12.002

Reiss, S., C. Harak, I. Romero-Brey, D. Radujkovic, R. Klein, A. Ruggieri, I. Rebhan, R. Bartenschlager, and V. Lohmann. 2013. The lipid kinase phosphatidylinositol-4 kinase III alpha regulates the phosphorylation status of hepatitis C virus NS5A. *PLoS Pathog.* 9:e1003359. http://dx.doi.org/10.1371/journal.ppat.1003359

Rocha, N., C. Kuijl, R. van der Kant, L. Janssen, D. Houben, H. Janssen, W. Zwart, and J. Neefjes. 2009. Cholesterol sensor ORP1L contacts the ER protein VAP to control Rab7–RILP–p150^{Glued} and late endosome positioning. *J. Cell Biol.* 185:1209–1225. http://dx.doi.org/10.1083/jcb.200811005

Rohde, H.M., F.Y. Cheong, G. Konrad, K. Paiha, P. Mayinger, and G. Boehmelt. 2003. The human phosphatidylinositol phosphatase SAC1 interacts with the coatomer I complex. *J. Biol. Chem.* 278:52689–52699. http://dx.doi.org/10.1074/jbc.M307983200

Rojas, R., T. van Vlijmen, G.A. Mardones, Y. Prabhu, A.L. Rojas, S. Mohammed, A.J.R. Heck, G. Raposo, P. van der Sluijs, and J.S. Bonifacino. 2008. Regulation of retromer recruitment to endosomes by sequential action of Rab5 and Rab7. *J. Cell Biol.* 183:513–526. http://dx.doi.org/10.1083/jcb.200804048

Rong, Y., M. Liu, L. Ma, W. Du, H. Zhang, Y. Tian, Z. Cao, Y. Li, H. Ren, C. Zhang, et al. 2012. Clathrin and phosphatidylinositol-4,5-bisphosphate regulate autophagic lysosome reformation. *Nat. Cell Biol.* 14:924–934. http://dx.doi.org/10.1038/ncb2557

Roth, M.G. 2004. Phosphoinositides in constitutive membrane traffic. *Physiol. Rev.* 84:699–730. http://dx.doi.org/10.1152/physrev.00033.2003

Roy, A., and T.P. Levine. 2004. Multiple pools of phosphatidylinositol 4-phosphate detected using the pleckstrin homology domain of Osh2p. *J. Biol. Chem.* 279:44683–44689. http://dx.doi.org/10.1074/jbc.M401583200

Salazar, G., B. Craige, B.H. Wainer, J. Guo, P. De Camilli, and V. Faundez. 2005. Phosphatidylinositol-4-kinase type II alpha is a component of adaptor protein-3-derived vesicles. *Mol. Biol. Cell*. 16:3692–3704. http://dx.doi.org/10.1091/mbc.E05-01-0020

Sarkes, D., and L.E. Rameh. 2010. A novel HPLC-based approach makes possible the spatial characterization of cellular PtdIns5P and other phosphoinositides. *Biochem. J.* 428:375–384. http://dx.doi.org/10.1042/BJ20100129

Schaletzky, J., S.K. Dove, B. Short, O. Lorenzo, M.J. Clague, and F.A. Barr. 2003. Phosphatidylinositol-5-phosphate activation and conserved substrate specificity of the myotubularin phosphatidylinositol 3-phosphatases. *Curr. Biol.* 13:504–509. http://dx.doi.org/10.1016/S0960-9822(03)00132-5

Schindelin, J., I. Arganda-Carreras, E. Frise, V. Kaynig, M. Longair, T. Pietzsch, S. Preibisch, C. Rueden, S. Saalfeld, B. Schmid, et al. 2012. Fiji: an open-source platform for biological-image analysis. *Nat. Methods*. 9:676–682. http://dx.doi.org/10.1038/nmeth.2019

Schmiedeberg, L., P. Skene, A. Deaton, and A. Bird. 2009. A temporal threshold for formaldehyde crosslinking and fixation. *PLoS ONE*. 4:e4636. http://dx.doi.org/10.1371/journal.pone.0004636

Schoebel, S., W. Blankenfeldt, R.S. Goody, and A. Itzen. 2010. High-affinity binding of phosphatidylinositol 4-phosphate by *Legionella pneumophila* DrrA. *EMBO Rep.* 11:598–604. http://dx.doi.org/10.1038/embor.2010.97

Shaner, N.C., R.E. Campbell, P.A. Steinbach, B.N.G. Giepmans, A.E. Palmer, and R.Y. Tsien. 2004. Improved monomeric red, orange and yellow fluorescent proteins derived from *Discosoma* sp. red fluorescent protein. *Nat. Biotechnol.* 22:1567–1572. http://dx.doi.org/10.1038/nbt1037

Sridhar, S., B. Patel, D. Aphkhazava, F. Macian, L. Santambrogio, D. Shields, and A.M. Cuervo. 2013. The lipid kinase PI4KIIIβ preserves lysosomal identity. *EMBO J.* 32:324–339. http://dx.doi.org/10.1038/emboj.2012.341

Stefan, C.J., A.G. Manford, D. Baird, J. Yamada-Hanff, Y. Mao, and S.D. Emr. 2011. Osh proteins regulate phosphoinositide metabolism at ER-plasma membrane contact sites. *Cell*. 144:389–401. http://dx.doi.org/10.1016/j.cell.2010.12.034

Suh, B.-C., T. Inoue, T. Meyer, and B. Hille. 2006. Rapid chemically induced changes of PtdIns(4,5)P2 gate KCNQ ion channels. *Science*. 314:1454–1457. http://dx.doi.org/10.1126/science.1131163

Szentpetery, Z., P. Várnai, and T. Balla. 2010. Acute manipulation of Golgi phosphoinositides to assess their importance in cellular trafficking and signaling. *Proc. Natl. Acad. Sci. USA*. 107:8225–8230. http://dx.doi.org/10.1073/pnas.1000157107

Tan, J., K. Oh, J. Burgess, D.R. Hipfner, and J.A. Brill. 2014. PI4KIIIα is required for cortical integrity and cell polarity during *Drosophila* oogenesis. *J. Cell Sci.* 127:954–966. http://dx.doi.org/10.1242/jcs.129031

Tóth, B., A. Balla, H. Ma, Z.A. Knight, K.M. Shokat, and T. Balla. 2006. Phosphatidylinositol 4-kinase IIIbeta regulates the transport of ceramide between the endoplasmic reticulum and Golgi. *J. Biol. Chem.* 281:36369–36377. http://dx.doi.org/10.1074/jbc.M604935200

Várnai, P., and T. Balla. 1998. Visualization of phosphoinositides that bind pleckstrin homology domains: calcium- and agonist-induced dynamic changes and relationship to myo-[^{3}H]inositol-labeled phosphoinositide pools. *J. Cell Biol.* 143:501–510. http://dx.doi.org/10.1083/jcb.143.2.501

Várnai, P., B. Thyagarajan, T. Rohacs, and T. Balla. 2006. Rapidly inducible changes in phosphatidylinositol 4,5-bisphosphate levels influence multiple regulatory functions of the lipid in intact living cells. *J. Cell Biol.* 175:377–382. http://dx.doi.org/10.1083/jcb.200607116

Wakana, Y., J. van Galen, F. Meissner, M. Scarpa, R.S. Polishchuk, M. Mann, and V. Malhotra. 2012. A new class of carriers that transport selective cargo from the trans Golgi network to the cell surface. *EMBO J.* 31:3976–3990. http://dx.doi.org/10.1038/emboj.2012.235

Walch-Solimena, C., and P. Novick. 1999. The yeast phosphatidylinositol-4-OH kinase pik1 regulates secretion at the Golgi. *Nat. Cell Biol.* 1:523–525. http://dx.doi.org/10.1038/70319

Wang, Y.J., J. Wang, H.Q. Sun, M. Martinez, Y.X. Sun, E. Macia, T. Kirchhausen, J.P. Albanesi, M.G. Roth, and H.L. Yin. 2003. Phosphatidylinositol 4 phosphate regulates targeting of clathrin adaptor AP-1 complexes to the Golgi. *Cell*. 114:299–310. http://dx.doi.org/10.1016/S0092-8674(03)00603-2

Watt, S.A., G. Kular, I.N. Fleming, C.P. Downes, and J.M. Lucocq. 2002. Subcellular localization of phosphatidylinositol 4,5-bisphosphate using the pleckstrin homology domain of phospholipase C delta1. *Biochem. J.* 363:657–666. http://dx.doi.org/10.1042/0264-6021:3630657

Weixel, K.M., A. Blumental-Perry, S.C. Watkins, M. Aridor, and O.A. Weisz. 2005. Distinct Golgi populations of phosphatidylinositol 4-phosphate regulated by phosphatidylinositol 4-kinases. *J. Biol. Chem.* 280:10501–10508. http://dx.doi.org/10.1074/jbc.M414304200

Yeung, T., G.E. Gilbert, J. Shi, J. Silvius, A. Kapus, and S. Grinstein. 2008. Membrane phosphatidylserine regulates surface charge and protein localization. *Science*. 319:210–213. http://dx.doi.org/10.1126/science.1152066

Zhu, Y., L. Hu, Y. Zhou, Q. Yao, L. Liu, and F. Shao. 2010. Structural mechanism of host Rab1 activation by the bifunctional *Legionella* type IV effector SidM/DrrA. *Proc. Natl. Acad. Sci. USA*. 107:4699–4704. http://dx.doi.org/10.1073/pnas.0914231107